Universidade de Aveiro   Departamento de Biologia

2019

Vera Cristina Martinho Pais

EFFECT OF CLASS I HISTONE DEACETYLASE INHIBITORS IN 3xTg-AD MICE

EFEITO DOS INIBIDORES DAS DEACETILASES DE HISTONAS DA CLASSE I EM MURGANHOS 3xTg-AD

DECLARAÇÃO

Declaro que este relatório é integralmente da minha autoria, estando devidamente referenciadas as fontes e obras consultadas, bem como identificadas de modo claro as citações dessas obras. Não contém, por isso, qualquer tipo de plágio quer de textos publicados, qualquer que seja o meio dessa publicação, incluindo meios eletrónicos, quer de trabalhos académicos.

Universidade de Aveiro Departamento de Biologia
2019

Vera Cristina Martinho Pais

EFFECT OF CLASS I HISTONE DEACETYLASE INHIBITORS IN 3xTg-AD MICE

EFEITO DOS INIBIDORES DAS DEACETILASES DE HISTONAS DA CLASSE I EM MURGANHOS 3xTg-AD

Dissertação apresentada à Universidade de Aveiro para cumprimento dos requisitos necessários à obtenção do grau de Mestre em Biologia Molecular e Celular, realizada sob a orientação científica da Prof. Doutora Ana Cristina Carvalho Rego, Professora Associada com Agregação da Universidade de Coimbra e da Prof. Doutora Virgília Silva, Professora Auxiliar do Departamento de Biologia da Universidade de Aveiro.

FCT
Fundação para a Ciência e a Tecnologia
MINISTÉRIO DA CIÊNCIA, TECNOLOGIA E ENSINO SUPERIOR

''Science is a willingness to accept facts even when they are opposed to wishes''

B.F. Skinner

o júri   Professor Doutor Mário Guilherme Garcês Pacheco

Professor Auxiliar com Agregação do Departamento de Biologia da Universidade de Aveiro

Professora Doutora Paula Isabel da Silva Moreira

Professora Auxiliar da Faculdade de Medicina da Universidade de Coimbra

Professora Doutora Ana Cristina Carvalho Rego

Professora Associada com Agregação da Faculdade de Medicina da Universidade de Coimbra

Agradecimentos

À Professora Doutora Ana Cristina Rego, por me ter acolhido no grupo, pela calma transmitida, pelo entusiasmo e pelas palavras confortantes nas alturas menos boas.

À Professora Doutora Virgília Silva, por ter aceitado ser minha orientadora durante este ano, pela disposição e pelo apoio dado.

À Ana Duarte, pelo maravilhoso acompanhamento durante este ano, por toda a força, ensino, experiência, pela confiança e principalmente pela amizade. Muito obrigada!

À Lígia, pela paciência, ajuda, confiança e pela partilha tão boa de pequenos momentos como ir só ao café. Obrigada por teres sido um dos maiores pilares do ano!

À Rita, pelas mensagens enormes a chatear-me a cabeça quando estou em stress, pelos jantares em casa, pela amizade e por todo o apoio dado neste meio ano.

A todo o grupo MNDlab, pelos bons momentos, pelo ensino profissional, pela partilha de conhecimento, pelos conselhos e ideias. Em especial à Patrícia, pela amizade, experiência partilhada e histórias contadas, muito obrigada por tudo! À Margarida e Carla, pela simpatia e prontidão a ajudar sempre. À Sandra, pelos conselhos e ajuda destes últimos tempos! Ao Rodolfo pelas palavras de apoio. À Luísa pela ajuda oferecida no início do meu percurso.

À Marisa, pelo ensino e prontidão a ajudar sempre que necessário.

À Elisabete pelo carinho, paciência e partilha de conhecimento e histórias.

Às meninas da Ana, Débora e Inês, pelos almoços, partilhas de histórias e amizade.

À Sara e Joana, pela amizade que espero que eterna!

Aos amigos da licenciatura de Bioquímica, principalmente à Sónia, Jéssica e Mara. Obrigada pelo apoio meus amores, por nunca me terem abandonado e por estarem sempre presentes mesmo afastadas! À Bea.

Aos colegas de mestrado de BMC, em especial ao Oldair. À Mariana e Bárbara, pela amizade criada durante o ano que passou e que continua, mesmo longe, pelas palavras de apoio, por serem chatas e pela paciência!

À melhor amiga do mundo, Flávia. Por nunca me abandonares, por todo o apoio e por levares contigo a nossa amizade para o resto da vida. Obrigada!

Ao Nuno, o melhor namorado do mundo! Obrigado pelos jantares, almoços, lanches e marmitas preparadas. Obrigado por saíres de casa só para me ires levar a mala do ginásio ao laboratório. Obrigado por aturares o meu mau feitio todas as vezes que chegava a casa chateada. Obrigada por me ouvires falar (sem parar) e nunca interromperes, ao ponto de revirares os olhos de ''já não te posso ouvir''. Obrigado por todas as vezes que quis comer porcaria e tu disseste que 'sim'. Obrigado pelo apoio deste ano, por acreditares em mim e nas minhas capacidades. Sem dúvida que sem ti tinha desistido. Amo-te!

Às pessoas mais importantes da minha vida, mãe, pai e avô. À mãe pelas oportunidades que me deu, pelo apoio, sacrifícios, por ser chata e por ser a melhor mãe do mundo. Ao meu pai, pelo apoio e palavras motivadoras! Ao meu avô, por tornar este último ano possível em Coimbra e por ser o mais atencioso do mundo. Às minhas duas estrelinhas. O maior obrigado do mundo é para vocês cinco!

Obrigada à família.

Palavras-chave

Doença de Alzheimer, deacetilases de histonas, butirato de sódio, murganho 3xTg-AD

Resumo

A doença de Alzheimer é a forma mais comum de demência a nível mundial. Clinicamente, caracteriza-se por declínio cognitivo, alterações de personalidade e humor, e desorientação. Neuropatologicamente, esta doença neurodegenerativa caracteriza-se pela acumulação extracelular do péptido beta-amilóide (βA), com formação de placas senis, e pela acumulação intracelular da proteína Tau hiperfosforilada formando tranças neurofibrilares. A patologia afeta maioritariamente o hipocampo, podendo progredir para o córtex cerebral. Estudos recentes mostram que a desregulação da acetilação das histonas está associada ao aumento da compactação da cromatina, com a consequente diminuição da transcrição génica. Assim, o estudo dos inibidores de enzimas que promovem a deacetilação das histonas, as HDAC (do inglês *histone deacetylase*), tem vindo a ganhar interesse como potenciais terapias contra a doença de Alzheimer. Para além disto, o péptido βA induz a produção de espécies reativas de oxigénio (ERO), tais como o peróxido de hidrogénio (H_2O_2), que promovem a atividade do fator de transcrição Nrf2 (do inglês *nuclear factor erythroid 2-related factor 2*), alterando assim a resposta antioxidante. Nesta perspetiva, neste estudo pretendemos avaliar o efeito de um inibidor das HDAC, o butirato de sódio (SB, do inglês *sodium butyrate*) (1 mg/kg/dia, durante 42 dias), na modificação dos sintomas e neuropatologia associados à doença de Alzheimer, utilizando o murganho triplo transgénico para a doença de Alzheimer (3xTg-AD).

Os animais 3xTg-AD com 10.5 meses de idade apresentaram um nível elevado de ansiedade em comparação com animais não transgénicos (*wild-type,* WT), que não foi minimizado pelo tratamento com SB. Por outro lado, em testes comportamentais que permitem avaliar processos mnemónicos, como o labirinto em Y (*Y-maze*), o reconhecimento de novos objetos e o teste de deslocação de objetos, não se observaram alterações significativas nos animais 3xTg-AD. A determinação dos níveis de acetilação da histona H3, dos níveis da proteína Tau total e fosforilada, assim como os níveis de Nrf2 nestes animais, com recurso à técnica de *Western blotting* mostrou que não só não existiam diferenças entre os animais 3xTg-AD e animais controlo *wild-type*, como o tratamento dos animais 3xTg-AD com SB não afetou nenhum destes parâmetros. Para tentar explicar a inexistência de diferenças entre os animais 3xTg-AD e WT avaliou-se a presença de agregados de βA e de Tau hiperfosforilada por imunohistoquímica nos animais 3xTg-AD. Porém, não se verificou a presença de marcadores histopatológicos da doença nestes animais. A explicação mais provável para estes resultados poderá ser um atraso no desenvolvimento da doença causado pelo aparecimento mais tardio dos marcadores histopatológicos e das alterações comportamentais, como sugerido na literatura recente sobre este modelo transgénico.

Futuramente, será necessária a realização deste estudo num modelo animal que apresente uma progressão mais acelerada da patologia, nomeadamente no murganho transgénico APP/PS1.

Keywords

Abstract

Alzheimer's disease is the commonest form of dementia worldwide. Clinically, this neurodegenerative disorder is characterized by cognitive decline, changes in personality and mood, and disorientation. Neuropathologically, it is characterized by the extracellular accumulation of beta-amyloid peptide (Aβ) forming senile plaques, and the intracellular deposition of hyperphosphorylated Tau protein forming neurofibrillary tangles. Alzheimer's disease affects primarily the hippocampus and may progress towards the cerebral cortex. Recent studies showed that deregulation of histone acetylation is associated with increased chromatin compaction and the subsequent decrease in gene transcription. Thus, the study of inhibitors of enzymes that promote histone deacetylation, HDACs (Histone DeACetylases) became a matter of interest in Alzheimer's disease therapeutics. Besides, it was shown that Aβ peptide induces the production of reactive oxygen species (ROS), such as hydrogen peroxide (H_2O_2), that further promote the activity of the Nrf2 (nuclear factor erythroid 2-related factor 2) transcription factor, altering cellular/tissue antioxidant profile. In this perspective, in this study we aimed to evaluate the possible effect of a HDAC inhibitor, sodium butyrate (SB) (1 mg/kg/day, for 42 days), in the attenuation of Alzheimer's disease-related symptoms and neuropathology, using the triple transgenic mice for Alzheimer's disease (3xTg-AD).

3xTg-AD mice at 10.5 months of age showed increased anxiety levels associated to the disease in comparison to non-transgenic/wild-type (WT) mice, that was not reverted by treatment with SB. Memory processes analysed through the Y-maze, the novel object recognition and object displacement tests showed no alterations in 3xTg-AD animals nor after treatment with SB. Quantification of acetylation levels of histone H3, the levels of total and phosphorylated Tau, as well as Nrf2 levels showed no significant differences between control and 3xTg-AD animals either. Treatment of 3xTg-AD mice with SB did not significantly affect any of these parameters either. Aiming to explain the lack of behavioural and biochemical differences between the 3xTg-AD and WT animals, the presence of Aβ aggregates and hyperphosphorylated Tau were assessed by immunohistochemistry in the hippocampus of 3xTg-AD mice. However, we did not observe any histopathological markers associated with this neurodegenerative disorder. The most probable explanation for these results is a delay in the disease development, leading to a later appearance of brain histopathological markers and behavioural alterations, as suggested by recent literature.

In future studies, it will be interesting to analyse an animal model with a more severe pathological progression, such as the APP/PS1 transgenic mice.

Contents

List of figures

List of tables

Abbreviations

˙OH- Hydroxyl radical

$O_2^{˙-}$- Superoxide anion

3xTg-AD- Triple transgenic animal model of Alzheimer's disease

AD- Alzheimer's disease

AICD- Amyloid intracellular domain

APP- Amyloid precursor protein

ARE- Antioxidant response element

ATP- Adenosine triphosphate

Aβ- β-amyloid peptide

BBB- Blood-brain barrier

CAT- Catalase

CSF- Cerebral spinal fluid

CT- Computed tomography

DNA- Deoxyribonucleic acid

DNMT- Deoxyribonucleic acid methyltransferase

FAD- Familial Alzheimer's disease

GCLM- Glutamate cysteine ligase

GPx- Glutathione peroxidase

GR- Glutathione reductase

GSH- Glutathione

GST- Glutathione transferase

fMRI- Functional magnetic resonance imaging

HAT- Histone acetyltransferases

HD- Huntington's disease

HDAC- Histone deacetylase

HDACi- Histone deacetylase inhibitor

KEAP1- Kelch-like ECH-associated protein 1

MAPT- Microtubule-associated τ protein

MCI- Mild-cognitive impairment

mRNA- messenger ribonucleic acid

miRNA- micro ribonucleic acid

MRI- Magnetic resonance imaging

MWM- Morris Water Maze

NAD$^+$- Nicotinamide adenine dinucleotide

NADPH- Nicotinamide adenine dinucleotide phosphate

Neh- Nrf2-ECH homology

NFT- Neurofibrillary tangles

NQO1- NAD(P)H: quinone oxidoreductase 1

Nrf2- Nuclear factor erythroid 2 related factor 2

NOR- Novel object recognition

OD- Object displacement

HO-1- Heme oxygenase 1

OF- Open field

pTau- Phosphorylated Tau

PB- Phenylbutyrate

PBA- 4-Phenylbutyrate

PBMC- Peripheral blood mononuclear cell

PET- Positron emission tomography

PKC- Protein kinase C

pNrf2- Nuclear factor erythroid 2 related factor 2 phosphorylated

PS1- Presenilin 1

PS2- Presenilin 2

PTM- Post-transcriptional modifications

RNA- Ribonucleic acid

ROS- Reactive oxygen species

SAD- Sporadic Alzheimer's disease

sAPPα- Soluble form of APP

SB- Sodium butyrate

SOD- Superoxide dismutase

TFs- Transcription factors

TSA- Trichostatin A

VPA- Valproic acid

WT- Wild-type

YAC128- Yeast artificial chromosome 128

CHAPTER I- Introduction

1. Alzheimer's disease

1.1 Epidemiology

Dementia is one of the major causes of disability in age-dependent human brain diseases. Alzheimer's disease (AD) is a progressive neurodegenerative disorder and the most common form of dementia (Maloney and Lahiri, 2011). Currently, AD is the most frequent cause of dementia in Western societies (Mayeux and Stern, 2012).

According to the World Alzheimer Report of 2018, 50 million people in the world live with dementia, a value that will duplicate by 2030 and triplicate by 2050. Thus, by 2050 about 152 million people are anticipated to suffer from dementia. These drastic figures stem from the fact that the population is becoming increasingly aged, due to the improvement in the health systems at world level, strongly contributing to an increase in life expectancy. Although elderly people are most of the AD-affected population, it is noteworthy that dementia is not a natural or normal part of aging, but a neurodegenerative condition that accentuates with aging. Between 2011 and 2013, the average life expectancy at birth of the resident population in Portugal was 80 years, an increase of approximately 3 years, compared to the previous decade (Santana et al., 2015).
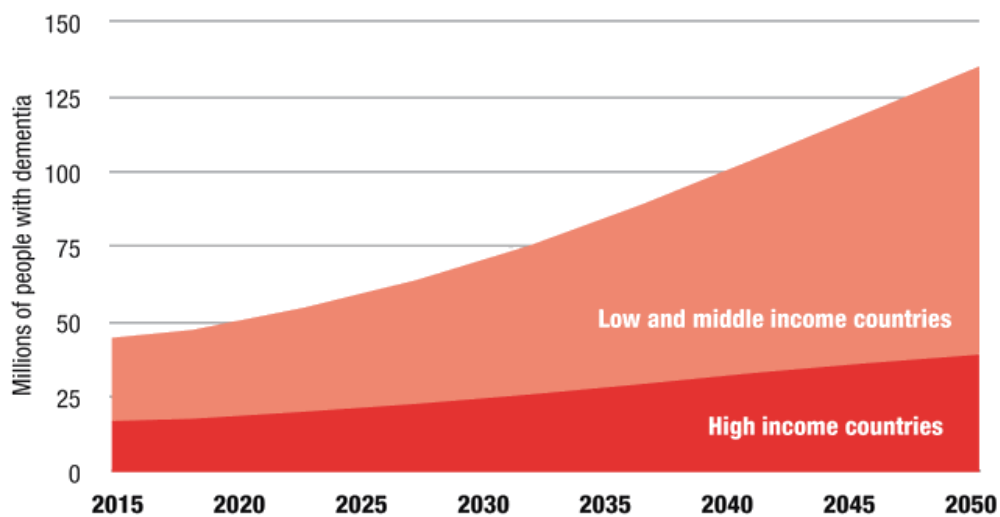
Figure 1- The growth in the number of people with dementia in high-, low- and middle-income countries. Source: World Alzheimer Report, 2015.

1.2 Forms and stages of AD

AD can be divided in two types: familial Alzheimer's disease (FAD) and sporadic Alzheimer's disease (SAD) (Masters et al., 2015). Familial forms of AD usually occur before the age of 65 and accounts for only 1% of AD cases (Chen et al., 2013b); AD-related mutations can affect one of three genes, amyloid precursor protein (APP), presenilin 1 (PS1) and presenilin 2 (PS2) (Reitz and Mayeux, 2014; Masters et al., 2015). SAD is the most common form of AD and usually manifests after the age of 65 (Khemka et al., 2015). The aetiology of this sporadic form is very limited, but several risk factors have been identified, such as aging and specific cardiovascular diseases (Bekris et al., 2010). Because the burden of SADs increases with age, many researchers have postulated that oxidative stress may be involved in the process of aging.

AD patients are clinically subdivided into four stages as mild cognitive impairment (MCI), mild, moderate and severe AD (Park and Moon, 2016). In the first stage, a person may represent amnestic symptoms or problems of concentration, such as forgetting familiar words or the location of everyday objects (Selkoe and Schenk, 2003). The second stage (moderate stage) can last for many years, dementia symptoms are more pronounced, and the person may have difficulty performing everyday tasks. In the third stage (late stage), dementia symptoms are severe. People are completely dependent on caregivers because they lose the ability to respond to their environment and to communicate (Lancet, 2011).

Histopathologically, both FAD and SAD forms are identical, both being characterized by brain atrophy and by the presence of amyloid plaques and neurofibrillary tangles (NFT) (Reddy, 2006; Masters et al., 2015). Under normal conditions there is a balance between the production and degradation of β-amyloid peptide (Aβ), in order to avoid its accumulation. With aging, Aβ levels in the brain as well as the degree of lesions associated with Tau protein begin to increase (**Figure 2**). In addition to these, brain atrophy and memory decline are also already visible factors in this state. Patients with MCI corresponds to a degree of cognitive impairment in memory, function or language (Albert et al., 2011). After several years of progressive memory decline, patients begin to experience deficits in motor function, disorientation, memory impairment and global cognitive deficits. As the severity of the disease increases, Aβ levels in the cerebrospinal fluid (CSF) decrease, as a result of the aggregation of the peptide in the brain, while Tau and phosphorylated Tau

(pTau) levels increase in the CSF (Tarawneh and Holtzman, 2012; Khemka et al., 2015). Brain atrophy as well as memory deficit are also increased on a large scale, facilitating the diagnose of AD.
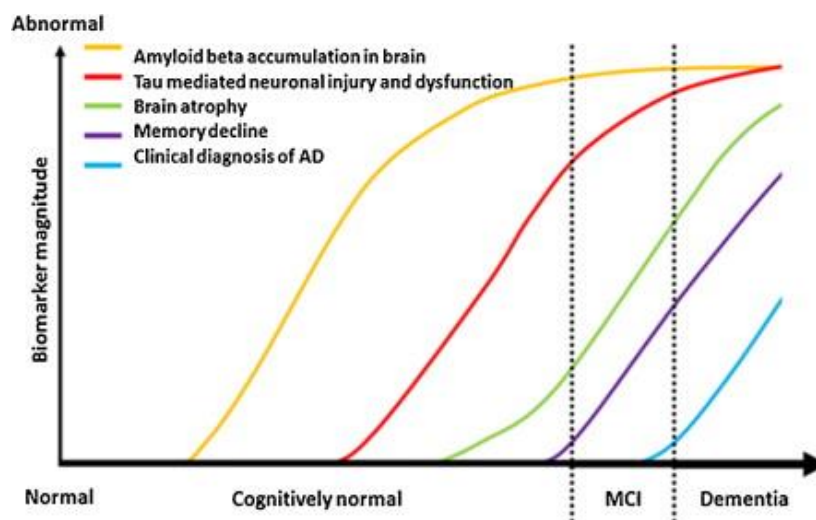
Figure 2- Towards defining a preclinical stage of AD. Taken from http://www.gepezz.info/similar/mild-cognitive-impairment-sciencedirect.html.

1.3 Causes of AD and risk factors

The major risk factor for the development of AD is age (Guerreiro and Bras, 2015); indeed, most cases of AD are observed in people aged 65 years or older (Chen et al., 2013a). Between 65 and 74 years of age, approximately 1% of people have AD, mostly corresponding to FAD; in people older than 85 years, the risk increases to 50%. In addition to aging, there are other factors associated with an increased risk for AD, such as cardiovascular disease, stroke, cerebral haemorrhage, hypertension, smoking, hyperglycemia and obesity (**Table 1**) (Khan et al., 2016). These factors decrease the quality of reasoning, memory, language, as well as emotional control.

Hypertension and cholesterol increase the risk of developing AD potentially due to the damage in blood vessels in the brain, causing less blood flow and death of brain tissue (Torre, 2012). Another risk factor in SAD is hyperglycemia linked to type II diabetes, which may be linked to partial or complete insulin resistance, leading to brain neuronal damage (Chen et al., 2009; Querfurth and LaFerla, 2010).

Table 1- Factors that modify the risk of AD. Adapted from (Khan et al., 2016)

Risk factor	Possible mechanisms
Cardiovascular disease	↑ Aβ deposition
Smoking	Cerebrovascular effects Oxidative stress
Hypertension	Microvascular disease
Type II diabetes	Cerebrovascular effects Insulin and Aβ compete for clearance
Obesity	Increased risk of type II diabetes inflammatory
Traumatic head injury	↑ Aβ and APP deposition

The clinical diagnosis of AD is usually performed through the assessment of signs and symptoms in the patient, such as memory loss and difficulty caring for oneself. For an accurate diagnosis it is necessary to examine brain tissue, however, a combination of different clinical evaluations such as mental, behavioral and physical tests, and radiological methods, may be applied (Mayeux, 2004; Taipa et al., 2012).

The first step in a diagnosis is to assess the patient's history. It is necessary to determine what symptoms are present, when they started and how they progressed over time. Physical examinations are also performed, including blood, CSF and urine tests. These analyses are very important because they will allow the identification of Aβ and pTau levels, two biomarkers of AD in the CSF (Albert et al., 2011). Structural imaging tests are also useful, including magnetic resonance imaging (MRI) and computed tomography (CT), which provide information about the shape and volume of the brain. Functional magnetic resonance imaging (fMRI) or positron emission tomography (PIB-PET) may also be used to complement the morphological studies (Jack Jr et al., 2010; Albert et al., 2011). However, only patients with persistent or progressive loss complaint of memory, confusion and difficulty performing standard cognitive tests may undergo imaging tests. The level of precision for diagnosis of AD is high because the disease can develop due to genetic,

environmental or lifestyle factors; imaging tests and biomarkers can be performed thus allowing a possible AD diagnosis (Mayeux, 2004; Dubois et al., 2007).

1.4 Pathology of AD

The clinical hallmarks of the disease are memory loss, cognitive impairment and altered language, visuospatial skills, executive function and personality (Hardy, 2006; Maloney and Lahiri, 2011), most probably related with irreversible loss of neurons in the hippocampus, progressing to the cortex.

The pathological hallmarks are the presence of neuritic plaques (**Figure 3A**), which are predominantly composed of Aβ peptide and NFTs (**Figure 3B**), composed of hyperphosphorylated microtubule-associated Tau (τ) protein (MAPT) (Oddo et al., 2003).
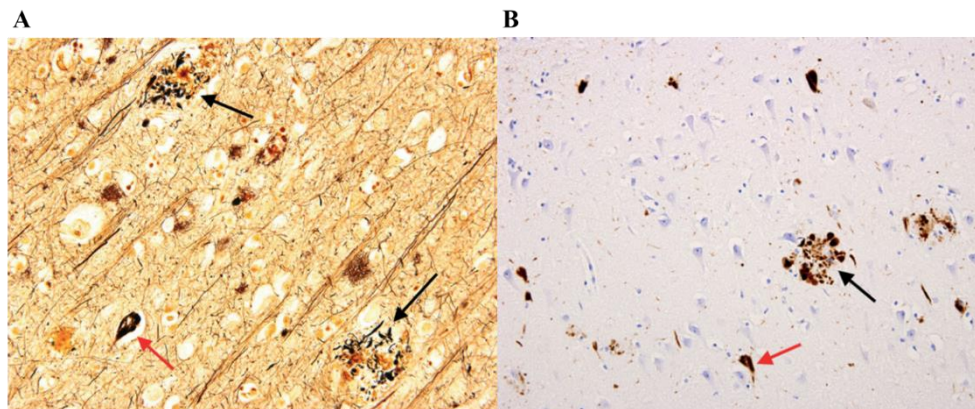
Figure 3- Pathological hallmarks of AD. Numerous neuritic plaques (black arrows) (**A**) and neurofibrillary tangles (NFT) (red arrows) (**B**). Adapted from (Perl, 2010)**.**

1.4.1 Production of amyloid-beta peptide

APP is a type 1 membrane glycoprotein that plays an important role in a range of biological activities such as signaling, intracellular transport and neuronal development. Aβ peptide results from the processing of APP (Chen et al., 2017). There are two proteolytic processing pathways of APP (**Figure 4**). In the nonamyloidogenic pathway, APP is initially cleaved by the α-secretase leading to the production of soluble form of APP (sAPPα) and a carboxyl-fragment (C83). Subsequently, the C83 fragment is cleaved by ɣ-secretase, producing the intracellular domain of APP (AICD) (Barage and Sonawane, 2015). In the amyloidogenic pathway, APP is cleaved by β-secretase and releases the large extracellular domain of APP, generating a C-terminal fragment composed by 99 residues (C99), that is

then cleaved by γ-secretase within the transmembrane domain to produce Aβ and AICD (Chen et al., 2013a, 2017).
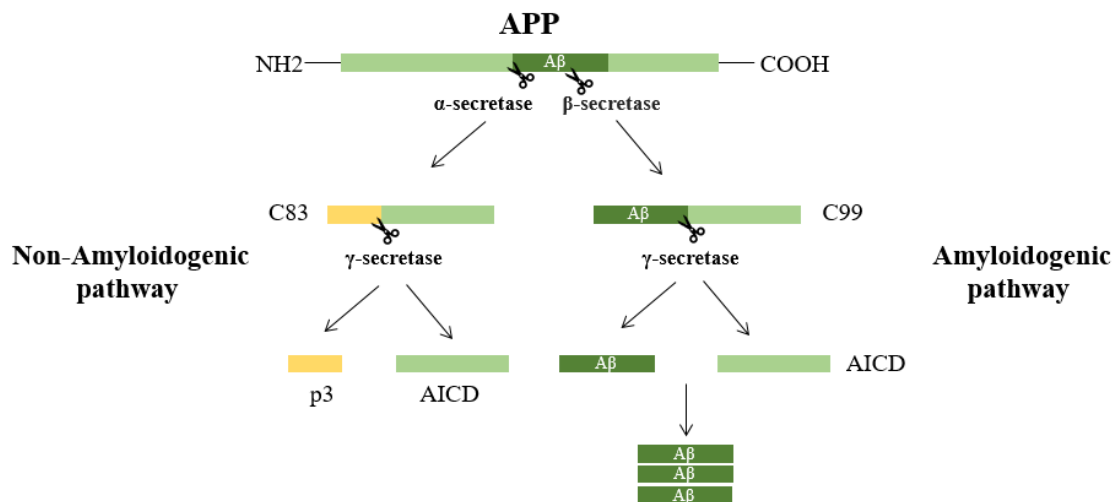
Figure 4- Proteolytic processing of APP in amyloidogenic and non-amyloidogenic pathways. α and γ secretases are responsible for the APP cleavage in the non-amyloidogenic pathway and in the amyloidogenic pathway β and γ secretases are involved. Adapted from (Sumner et al., 2018).

Changes in APP processing such as those linked to PS1 and 2 (components of complex of γ-secretase complex) are linked to the overproduction of Aβ (Bekris et al., 2010; Maloney and Lahiri, 2011). Aβ peptides exhibit 36-43 amino acids that can agglutinate and form amyloid aggregates, found primarily in aged neurons (Zuo et al., 2015). In addition, it exhibits the ability to self-aggregate in different forms such as oligomers, Aβ40 and Aβ42, the more toxic species for cells (Cheignon et al., 2018). The Aβ40 is the most common form of Aβ in the brain, but Aβ42 is the most toxic, being considered the primarily Aβ form responsible for neuronal damage (Gu and Guo, 2013). Since these oligomers are soluble and toxics, their accumulation and aggregation leads to the formation of neuritic or senile plaques (Bordon, 2017). The neurodegeneration associated with AD is characterized by loss of synaptic function (Magalingam et al., 2018), inflammation and synaptotoxicity (Kocahan and Doğan, 2017) that results in gradual neuronal death and memory loss, through the interruption of neuronal communication.

1.5 The Amyloid Cascade Hypothesis

The amyloid cascade hypothesis was formulated in 1990s and has become a dominant model for AD pathogenesis (Swerdlow, 2007). According to this hypothesis, there is an abnormal increase of Aβ levels that leads to Aβ aggregation into β-sheet rich structures (Cheignon et al., 2018). The Aβ peptides, which are not degraded by cells, can form oligomers and Aβ fibrils, being able to permeabilize the membrane and represent a primary mechanism of amyloid pathogenesis (Glabe, 2006). Thus, Aβ participates or contributes to neuronal dysfunction, neurotoxicity, cell death and overproduction of reactive oxygen species (ROS) (Zuo et al., 2015). In addition, the oxidative stress may also induce increased levels of Aβ and pTau, leading to the onset and progression of AD.

The increase in Aβ42 levels enhances oligomers formation (**Figure 5**), being responsible for local inflammatory responses such as microgliosis and astrocytosis (Frost and Li, 2017). Consequently, oxidative stress and neuronal injury lead to synaptic and neuritic loss. Those processes culminates with cell death, leading to progressive dementia associated with extensive Aβ and Tau pathology (Ricobaraza et al., 2010; Barage and Sonawane, 2015).
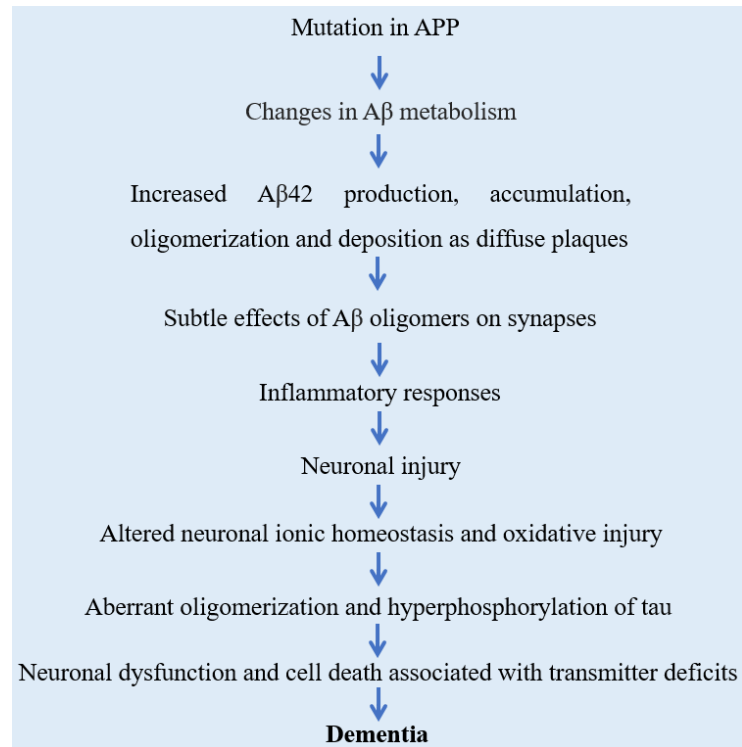
Figure 5- **The amyloid cascade hypothesis.** This hypothesis proposes that an abnormal increase of Aβ levels leads an accumulation of senile plaques, an initial pathological event in AD. Together with hyperphosphorylated Tau exists an increase of accumulation of ROS that starts an inflammatory response, resulting in neuronal death and causing AD. Adapted from (Hardy and Selkoe, 2002).

However, in recent years, this hypothesis has been reappraised. The importance of Aβ fibrils has been questioned because the number of Aβ plaques is not correlated to the severity of disease (Hardy and Selkoe, 2002; Barage and Sonawane, 2015). Aβ plaques are also found in healthy humans and with a similar composition, which implies that other factors are involved in AD. Therefore, this hypothesis was directed to smaller forms of Aβ (Armstrong, 2014), the Aβ oligomers. The oligomers were considered the main causing agents for pathological alterations in AD and were associated with neurotoxic activities because of the high soluble Aβ concentrations in the brain contributing to neurodegeneration in AD (McLean et al., 1999; Serrano-Pozo et al., 2011). However, these oligomers are not the only ones that derive from the processing of APP, since other fragments are produced during its cleavage by secretases (**Figure 4**) (Maloney and Lahiri, 2011; Chen et al., 2017). Thus, the peptide Aβ may not be the main pathogenic factor of the disease but is, at least, involved in its progression.

2. Oxidative stress and transcriptional changes in Alzheimer's disease

2.1 ROS and oxidative stress

ROS play very important roles in cell signalling, cell growth, synthesis of biological molecules and stress responses (Zuo et al., 2015). However, high levels of ROS in the cells cause modifications on several biomolecules such as proteins, lipids and deoxyribonucleic acid (DNA). In normal conditions, there is a constant production of ROS in the cells, however, oxidative stress is the result of an imbalance between the formation of ROS and their neutralization by the antioxidant defences (Ferreiro et al., 2012; González-Reyes et al., 2017). Mitochondrial oxidative phosphorylation is the major source of ROS, thus, when mitochondrial function is altered, ROS concentrations can be dramatically elevated. Some examples of ROS are hydrogen peroxide (H_2O_2), hydroxyl radical ($^{\bullet}OH$) and superoxide anion ($O_2^{\bullet-}$). The cell has enzymatic and molecular antioxidant defences to cope with the ROS production such as superoxide dismutase (SOD), heme oxygenase-1 (HO-1), glutathione peroxidase (GPx), glutaredoxins, thioredoxins and catalases (CAT) (Reddy, 2006).
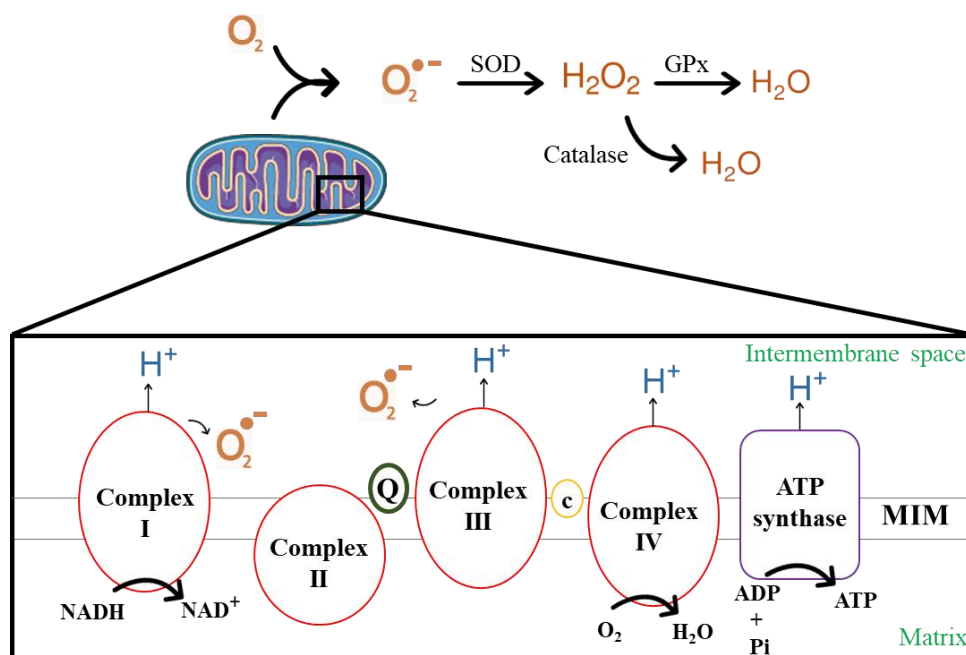
Figure 6- Formation of ATP and ROS. Mitochondrial electron transport is composed by three complexes: I, III and IV, while ATP synthase utilizes the proton motive force to synthesize ATP from ADP. Adapted from (Li et al., 2013)

Brain has high energy consumption and is highly susceptible to ROS damage. Thus, the balance between ROS production and the antioxidant defence system is essential for normal cellular function. However, in AD, the increase in oxidative stress accelerates to misfolding and aggregation of Aβ and pTau (González-Reyes et al., 2017; Fertan et al., 2019), causing cellular injuries and mitochondrial dysfunction (González-Reyes et al., 2017).

2.2 Antioxidant transcriptional factor – Nrf2

The activation of transcription factors (TFs) have an important role in oxidative stress neutralization. The levels of TFs in human postmortem brain and animal models of AD are reduced (Caldeira et al., 2013). However, it is unclear whether Aβ directly modulates gene expression by altering gene promoters or by interfering with the activity of TFs, in brain cells (Shi and Gibson, 2007; Barucker et al., 2014). Importantly, TFs can modulate mitochondrial biogenesis and function and the levels of antioxidant enzymes, thus reducing the harmful impact of ROS in cells. One of the most important TFs in ROS combat is the nuclear factor erythroid 2 related factor 2 (Nrf2) (Bahn and Jo, 2019).

Nrf2 has a crucial role in stress conditions, mediating the expression of antioxidant proteins, detoxifying enzymes and others TFs (Esteras et al., 2016) and contains seven conserved domains (**Figure 7**) (Esteras et al., 2016; Dinkova-Kostova et al., 2018; Bahn and Jo, 2019).
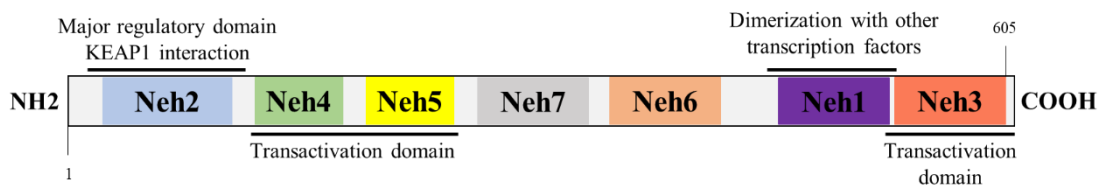
Figure 7- Structural domains of Nrf2 protein. Nrf2 protein consists of 605 amino acids and has seven homology domains, Neh1–7. The domains of interest in Nrf2 are: Neh2 domain, required for the interaction with KEAP1, and a hydrophilic region of lysine residues, which are indispensable for the Keap1-dependent polyubiquitination and degradation of Nrf2. Adapted from (Bahn and Jo, 2019).

Under basal conditions, Nrf2 is mostly located in cytoplasm where it can bind to Kelch-like ECH-associated protein 1 (KEAP1), its endogenous inhibitor, leading to Nrf2 ubiquitination and degradation by the ubiquitin-proteasome system, which act as an adaptor for Cullin-3-based E3 ubiquitin ligase complex (Canning et al., 2015). Following an increase

in ROS levels, KEAP1 is oxidized in its cysteine residues, which alters its conformation, leading to E3 ubiquitin ligase inhibition and releasing of Nrf2, which then translocate into the nucleus (Esteras et al., 2016). Nrf2 mediates the expression of proteins which genes contain a *cis* regulatory element named "antioxidant response element" (ARE). In the nucleus, Nrf2 heterodimerizes with Maf proteins and the heterodimers bind to AREs to regulate the transcription of Nrf2 target genes, such as SOD1, GPx, CAT and HO-1 (**Figure 8**) (Dinkova-Kostova et al., 2018; Bahn and Jo, 2019).
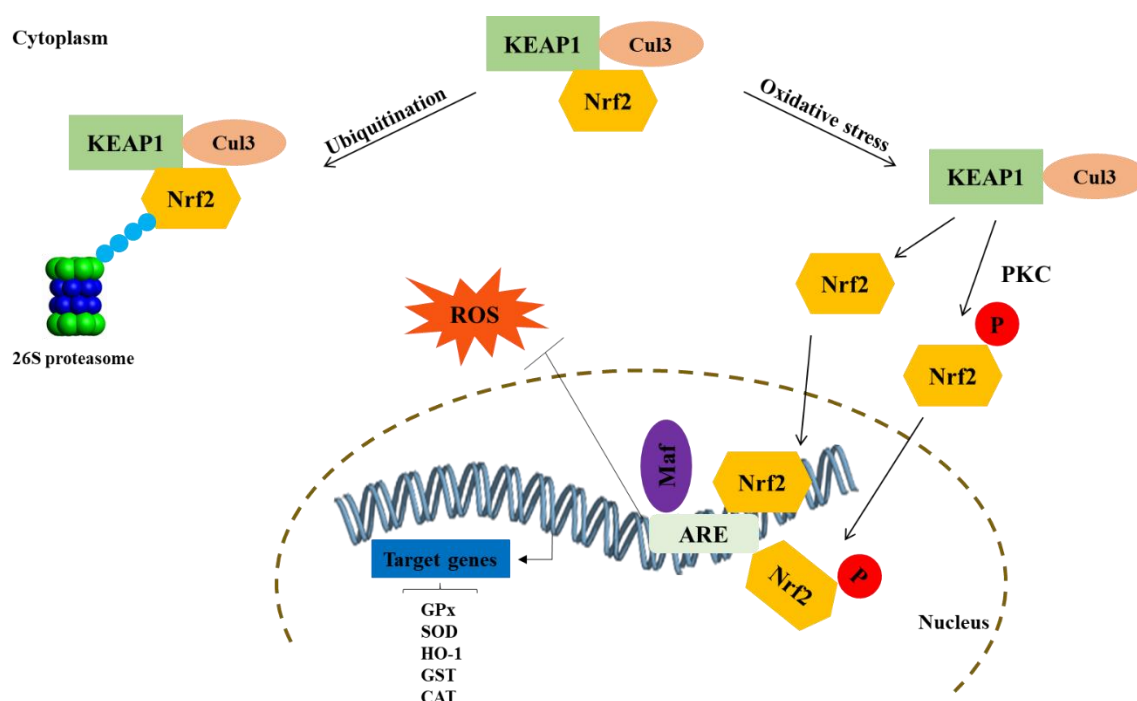
Figure 8- Schematic representation of the Nrf2/Keap1 intracellular pathway. Under normal conditions, KEAP1 inhibits Nrf2 signaling pathway, it is ubiquitinated and degraded by the proteasome. In the presence of ROS, Nrf2 dissociates from KEAP1, leading to translocation of Nrf2 into nucleus. In these same conditions, the Nrf2 phosphorylation by PKC occurs, resulting in Nrf2 nuclear translocation. In the nucleus, Nrf2 promotes transcriptional activation of antioxidants and detoxifying enzymes by binding to the ARE in the promoter regions of the target genes. Adapted from (Nicoletti et al., 2014) and (Sova and Saso, 2018).

Additionally, it has been shown that phosphorylation of Nrf2 (pNrf2) contributes to its nuclear migration (Caldeira et al., 2013), since Nrf2 contains serine, threonine and tyrosine residues, which can be sites for phosphorylation by different kinases (Sun et al., 2009). Phosphorylation of Nrf2 at Ser40 residue by protein kinase C (PKC), impairs its association with KEAP1 thus promoting its activation and translocation to the nucleus (**Figure 8**) (Fão et al., 2019). This phosphorylation may be necessary for the dissociation of

Nrf2 from KEAP1 and for Nrf2 nuclear migration. Taking this into account, Nrf2 has been described to be a promising target for therapeutic strategies in the context of neurodegeneration because it regulates the expression of cytoprotective and antioxidant enzymes.

2.2.1 Nrf2 in Alzheimer's disease

Some early studies in both human and animal models show that Nrf2 levels in AD are decreased when compared to healthy individuals, suggesting a decrease in Nrf2 activity (Vasconcelos et al., 2019). Consequently, some enzymes regulated by Nrf2 have decreased activity such as SOD1, glutathione (GSH), CAT (Ansari and Scheff, 2010) and glutathione transferase (GST) (Lovell et al., 1998) in human AD cortex, however, the activity of NAD(P)H:quinone oxidoreductase 1 (NQO1) (Raina et al., 2004), glutathione reductase (GR), GPx (Johnson and Johnson, 2015) and HO-1 (Schipper et al., 1995) is increased, in human AD brain. A study of Nrf2 in APP/PS1 animal model showed no differences in NQO1 and glutamate cysteine ligase (GCLM) messenger ribonucleic acid (mRNA) levels but a decrease in GCLM and NQO1 expression at 6 months-old and a reduction in Nrf2 levels at 16 months of age (Kanninen et al., 2008). More recently, APP/PS1 mice at 7-8 months-old showed increased levels of OH-1 and GPx, however mRNA levels of GCLM and NQO1 were not altered (Joshi et al., 2015). Concordantly, the triple transgenic animal model of AD (3xTg-AD)animal model showed increased NQO1 and augmented Nrf2 and SOD protein levels in both hippocampus and cortex, at 2 months and 3 months of age, respectively (Mota et al., 2015). Conversely, decreased SOD1 and HO-1 mRNA were also found at 3 months of age. However, at 6 and 15 months-old, this model showed reduced NQO1 and Nrf2 levels in the hippocampus (Torres-Lista et al., 2014) (Mota et al., 2015). Additionally, some studies show that at 3-month-old 3xTg-AD mice, Nrf2 phosphorylation levels at Ser40 are increased in peripheral blood mononuclear cells (PBMCs) and the nuclear levels of Nrf2 are decreased in the brain cortex. Accordingly, an increase in oxidative stress levels, as well as phosphorylation of Nrf2, were found in PBMCs of humans with MCI (Mota et al., 2015). However, in both 3xTg-AD mice and human PBMCs, it was found that SOD1 protein levels were decreased, suggesting a failure in the regulation of Nrf2 target genes in AD.

These distinct results may be explained by different levels of Nrf2 at different stages of the disease and the type of tissue collected for the study, perhaps indicative of a positive

regulation of antioxidant defenses to combat oxidative stress in the early stages of AD, whereas the loss of antioxidant enzyme activity as well as the Nrf2/ARE pathway may be more evident in the later stages of the disease (Sun et al., 2017).

3. The triple transgenic Alzheimer's disease mouse model

There are several transgenic animal models of AD that mimic some of the hallmarks described in human patients and that are used in research for understanding the disease mechanisms and development of therapeutic treatments. The triple transgenic AD mouse model (3xTg-AD) (**Figure 9**) exhibits the behavioural and neuropathological (neuritic plaques and neurofibrillary tangles) changes that are observed in AD patients (Oddo et al., 2003).

Figure 9- 3xTg-AD mouse model. Taken from https://www.jax.org/strain/004807

The 3xTg-AD mouse was first described by Oddo et al. (2003). It expresses three human mutant genes: $PS1_{M146V}$, $APP_{K670N/M671L}$ (also named APP_{Swe}), and Tau_{P301L} (**Figure 10**). This transgenic line was created by microinjection of two transgenes: APP_{Swe} and Tau_{P301L} into single-cells from homozygous $PS1_{M146V}$ knock-in mice.
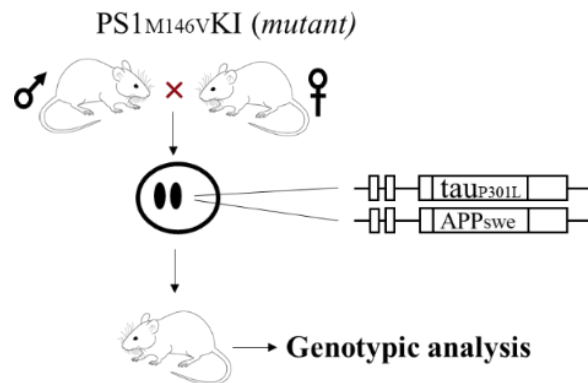
Figure 10- Strategy used to develop the 3xTg-AD mice. Adapted from (Oddo et al., 2003).

In this mouse model, intraneuronal Aβ plaques appear first between 3 and 4 months of age in the neocortex and by 6 months of age in hippocampal CA1 pyramidal neurons. Extracellular deposits of Aβ first appear in 6 months-old mice in the frontal cortex and expand to the hippocampus at 12 months of age. Tau pathology appears after 12 months of age, particularly in hippocampal neurons.

In general, 3xTg-AD mice demonstrated decrease exploratory activity and higher anxiety levels and depression such as in AD human (Stover et al., 2015; Huber et al., 2018). According to the behavioural and cognitive characterization performed by Sterniczuk, 3xTg-AD females between 7.5 and 11 months of age presented high levels of anxiety (Sterniczuk et al., 2010b) and depression. In this model, there is a rapid decline in cognitive ability, the capacity of learning and memory is also affected.

4. Protein acetylation and epigenetic alterations in Alzheimer's disease

4.1 Epigenetic alterations and transcription regulation

Epigenetic changes consist in altering the expression of genes without affecting the DNA sequence, as a result of environmental stimuli, growth or development (Zuo et al., 2015). Epigenetic alterations can be described as three main mechanisms: DNA methylation, histone modifications and microRNA (miRNA) activity. DNA methylation can be described as the addition of a methyl (CH_3) group by DNA methyltransferase (DNMT) enzyme to the cytosines that precede the guanines, inactivating transcription by preventing the binding of TFs (Yin et al., 2017). Histone modifications involve acetylation, methylation, phosphorylation or ubiquitylation of histones. In histone modification, chromatin remodelling was identified as the major epigenetic mechanism because this modification has

important roles in transcriptional regulation (Gräff et al., 2011; Sanchez-Mut and Gräff, 2015). miRNAs are the most studied group of noncoding RNAs and are negative regulators of gene expression at the posttranscriptional level (Qiu et al., 2015; Cao et al., 2018). These regulate different physiological functions such as growth, development and cellular homeostasis. About 70% of miRNAs have been detected in the brain (Sharma and Lu, 2018) and therefore have a high importance in synaptic development, neuroplasticity as well as in the formation and maturation of synapses. Curiously, miRNA expression is altered in AD (Qiu et al., 2015).

The nervous system is a highly specialized system where cells are organized in different sub-structures, with different epigenetic profiles (Cao et al., 2006). Thus, neuronal activity and brain function are regulated by a dynamic modulation of chromatin and gene expression profiles, namely after histone post-translational modifications (PTM).

4.2 Histone modifications – acetylation *vs*. deacetylation

Histones are the most abundant proteins associated with DNA and their acetylation is the most studied modification. It involves the transfer of an acetyl group from acetyl coenzyme A to lysine residues at the histone tails (Zovkic et al., 2013) by histone acetyltransferases (HAT), while histone deacetylases (HDAC) act to remove acetyl groups (**Figure 11**) (Delcuve et al., 2012; Sanchez-Mut and Gräff, 2015). In normal neurons, the protein levels of HAT and HDAC and their activities are kept in a balanced state, hence regulating normal gene expression (Xu et al., 2011). Recent studies suggest that the decrease in histone acetylation is associated with an increased compaction of chromatin (Zwergel et al., 2016) since the positive charge of modified histone protein, due to the amine group of its composition, facilitates interactions with negatively charged DNA and promotes condensed chromatin states, thereby repressing gene transcription (Sanchez-Mut and Gräff, 2015).
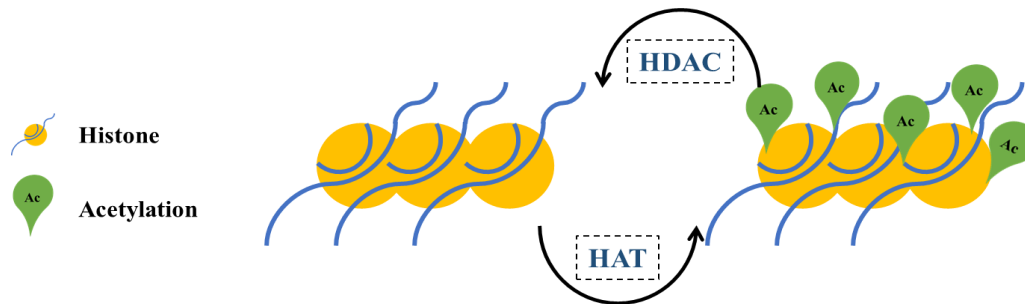
Figure 11- Modifications of histones by HATs and HDACs. HATs transfer acetyl groups to lysine residues of histones and gene transcription is activated, whereas HDACs remove acetyl groups from histones and gene transcription is inactivated. Adapted from (Schneider et al., 2013).

HDACs are divided into three zinc-dependent classes: class I, class II and class IV. There is also class III, which is dependent on nicotinamide adenine dinucleotide (NAD^+), as the sirtuins (Gräff et al., 2011). The zinc-dependent classes present different HDACs, as reported in **Table 2**.

Table 2- Classes of zinc-dependent HDACs and their preferential localization.

	Nucleus	**Cytoplasm**
Class I	1, 2, 3 and 8	-
Class IIa	4, 5, 7 and 9	4, 5, 7 and 9
Class IIb	-	6 and 10
Class IV	11	-

Histone acetylation occurs in the hippocampus in response to contextual learning (Levenson et al., 2004), however, this acetylation is disturbed in neurodegenerative states, because the levels of HAT activity are reduced (Pirooznia and Elefant, 2013). Previous studies (Ferrante et al., 2003; Fischer et al., 2007; Ricobaraza et al., 2009; Cao et al., 2018) aimed to characterize chromatin modifications in AD and they were mainly focused on HDACs, which when inhibited showed neuroprotective effects in AD animal models.

4.2.1 Class I of HDACs

Class I of HDACs consists of HDACs 1, 2, 3, and 8, which are mainly localized in the nucleus, where they regulate histone acetylation, HDAC8 is generally poorly expressed (Alaghband et al., 2017). The levels of HDAC1 mRNA were also lower when compared

with HDACs 2 and 3. Recent studies indicate that the activity of specific class I enzymes may be altered in psychiatric diseases and may play a role in the effective treatment (Xu et al., 2011). According to Guan and colleagues, the inhibition of HDAC2 results in an increase in synaptic plasticity, number of synapses and memory formation (Guan et al., 2009). Thus, they claim that this is a negative regulator of memory formation and syntactic plasticity (Gräff et al., 2011; Xu et al., 2011). HDAC1 and HDAC2 exhibit a degree of homology (Delcuve et al., 2012), however, the role of HDAC1 in memory is opposite to that of HDAC2 (Bahari-Javan et al., 2014). When HDAC3 levels are inhibited this enzyme has the ability to restore the synaptic plasticity induced by oligomers of Aβ in neurons (Krishna et al., 2016), so HDAC3 plays a negative role in memory formation. As HDCA8 is poorly expressed, information regarding its role in memory formation or neural plasticity is scarce (Delcuve et al., 2012).

4.3 Histone deacetylases inhibitors and their treatment in Alzheimer's disease

The HDAC inhibitor (HDACi) can be classified into different classes: fatty acids [sodium butyrate (SB), phenylbutyrate (PB) and valproic acid (VPA)]; hydroxamic acids [(trichostatin A (TSA) and SAHA)]; mercaptoketone (KD5170), cyclic peptides and benzamides [(tacedinaline (CI-994) and MS-275] (Tandon et al., 2016). Amongst these, the most widely studied are SB, PB, VPA, TSA and SAHA, a pan inhibitor of HDACs. In contrast, SB, PB and KD510 are selective to classes I and IIa HDAC (Fessler et al., 2013; Tandon et al., 2016). For class I HDACs, the inhibitors with better selectivity are MS-275, CI-994 and, finally TSA, which was the first discovered to inhibit HDACs (Yoshida et al., 1990), namely by inhibiting the activity of classes I and II HDACs.

Inhibition of class I HDAC isoforms simultaneously could be a promising therapy for improving transcriptional levels, promoting synapse formation and ameliorating cognition (Yang et al., 2017). These inhibitors are potential treatment for AD due to their effect on decrease of Aβ levels (Xu et al., 2011). In 2003, Hockly and colleagues showed that Varinostat (SAHA), an HDACi led to increased levels of histone acetylation when administered orally in drinking water, in the R62 mice model of HD (Hockly et al., 2003). With this, they have showed that HDACis can be used as a possible treatment strategy in neurodegenerative diseases and identified a neuroprotective mechanism that includes the

regulation of histone acetylation homeostasis. The HDACis increase the acetylation levels of histones by reducing deacetylation, subsequently upregulating gene transcription, and also enhance hippocampus dependent memory formation (Levenson et al., 2004; Guan et al., 2009; Zwergel et al., 2016).

It was demonstrated that HDACis are able to decrease Aβ levels in transgenic mice by targeting genes required for Aβ formation. For example, the use of VPA reduces Aβ plaques and restores memory in APP23 mice model (Qing et al., 2008). Similarly, SAHA was shown to rescue contextual memory in APP/PS1 model, to cross the blood-brain barrier (BBB) and to increase H4 acetylation in the brain (Kilgore et al., 2010). Moreover, the administration of MS-275 in the APP/PS1 mouse model caused a decrease in Aβ deposition and attenuated inflammatory (Zhang and Schluesener, 2013). Administration of the 4-phenylbutyrate (PBA) inhibitor in the animal model Tg2576 of AD (duration of 5 weeks) with 6 and 12-16 months, led to the restoration of memory as well as learning capacity (Ricobaraza et al., 2010). In addition, administration of SB intraperitoneally for 6 weeks in the 15-month APP/PS1-21 animal model allowed for memory restoration, increased expression of genes associated with learning as well as to the increase of histone acetylation (Govindarajan et al., 2011). The study of Zhang and colleagues, showed that MS-275 administered orally in APP/PS1 mice model for 10 days, led to a decrease in Aβ deposition in the cortex as well as in the hippocampus (Zhang and Schluesener, 2013). More recently, in YAC128 model of Hungtinton's disease (HD), the administration of SB (1 mg/kg/day) through mini-osmotic pumps, led to an increase in histone acetylation levels (Naia et al., 2017). These results suggest that, when used at low concentrations/doses, HDACis may constitute a therapeutic option in AD as well as in other neurodegenerative diseases since they are expected to have beneficial neuroprotective effects. More recently, in 2018, it has been shown by Janczura and colleagues that oral administration of RGFP-966, an inhibitor of HDAC3, led to decreased Aβ42 protein levels in the brain in the 3xTg-AD mouse model (Janczura et al., 2018).

In addition to these HDACis, previous studies with SB demonstrated neuroprotective effects, ameliorated oxidative stress and inflammation, and improved memory deficits in a mouse model of cerebral ischaemia (Sun et al., 2015). Furthermore, a prolonged treatment with SB also improved memory in APP/PS1 mice even in advanced stages of pathology, and increased the expression of genes implicated in learning (Govindarajan et al., 2011). Moreover, class I HDACis such as SB elevated histone H4 acetylation and restored contextual memory in the APP/PS1 mice model of AD (Kilgore et al., 2010; Xu et al., 2011). Therefore, increasing histone acetylation to ameliorate memory in the context of AD may be a promising therapeutic strategy.

CHAPTER II- Objectives

The presence of Aβ and intracellular neurofibrillary tangles constitute pathological hallmarks of AD. The balance between acetylation of histones by HAT and HDAC represents a central mechanism in regulation of gene expression (Xu et al., 2011). Deregulation of histone acetylation has been implicated in the onset of age-associated memory impairment and AD pathogenesis because the reduction in histone acetylation levels promotes amnesia and interferes with the consolidation of memories (Bahari-Javan et al., 2014). Moreover, the levels of Nrf2 are altered in this disease. The levels of histone acetylation is possible to modulate with specific HDACis (Cao et al., 2018).

Considering that AD has been characterized by impaired memory, cognition and personality, decreased acetylation of histones due to lower HAT and altered levels of Nrf2, the main aims of this work are:

I) To determine the impact of sodium butyrate on behavior profile of 3xTg-AD mice

In this study, 3xTg-AD mice with 10.5 months of age will be subjected to different behavioral tests for analysis of anxiety, cognition and memory in order to evaluate if treatment with the HDACi sodium butyrate (SB) affects these AD-related behaviors in 3xTg-AD, compared to untreated/saline-treated 3xTg-AD and wild-type (WT) mice;

II) To evaluate the influence of sodium butyrate on histone acetylation in the brain cortex of 3xTg-AD mice

The activity of histones can be controlled by inhibitors of HDACs. Therefore, we will evaluate the acetylation levels of H3 histone after treatment of 3xTg-AD mice with SB, compared to untreated/saline-treated 3xTg-AD and WT mice;

III) To examine the changes in Tau protein levels and phosphorylation, and protein levels of ROS-related transcription factor Nrf2 and phosphorylation following SB treatment in the brain cortex of 3xTg-AD mice

We will determine the levels of Nrf2 and pNrf2 in 10.5 months-old 3xTg-AD mice brain treated with SB, compared to untreated/saline-treated 3xTg-AD and WT mice.

CHAPTER III- Material and methods

Effect of class I histone deacetylase inhibitors in 3xTg-AD mice

3.1 Material

All materials and reagents were of the highest grade of purity commercially available. Sodium butyrate (SB), protease inhibitor cocktail, hydrogen peroxide (H_2O_2) and goat serum were from Sigma Aldrich (St Louis, Missouri). Mini-osmotic pumps were from Alzet (Durect Cop., Cupertino, California). Sodium pentobarbital was from Nephar - Farma lda, (Mem Martins – Portugal) and buprenorphine was from Laboratórios Karizoo, S.A. (Caldes de Montbui – Espanha). Fatty acid-free bovine serum albumin (BSA) used in Western Blotting was purchased from NZYtech (Lisbon, Portugal). BioRad Protein Assay was purchased from BioRad Laboratories, Inc. (Munich, Germany), Western Blot Immobilon-℗ PVDF membrane, and phenylhydrazine and Triton-X100 used in immunohistochemistry were from Merck Millipore (Darmstadt, Germany). Tissue-Tek optimum cutting temperature (O.C.T.) cryostat sectioning medium was from Sakura Finetek (United Kingdom). Toluene-based Richard-Allan Scientific Mounting Medium and DPX Mounting Medium were from Thermo Scientific (Waltham, Massachusetts, EUA). Hoechst 33342 nucleic acid stain was purchased from Invitrogen/Molecular Probes (Life Technologies Corporation, Carlsbad, CA, USA). Cryostat-microtome Leica CM3050S was from Leica Microsystems Nu (Wetzlar, Germany) and microscope Zeiss Axio Imager Z2 microscope were from Zeiss (Oberkochen, Germany). All the primary antibodies used for Western Blotting and immunohistochemistry are described in **Table 2** and **Table 4**, respectively.

Table 3- Antibodies used for Western Blotting analyses.

Primary antibodies	Host	Dilution	Reference
Tau-5	Mouse	1-2 µg/mL	Abcam (#ab80579)
Phospho-Tau (T231)	Rabbit	1:5000	Abcam (#ab151559)
Acetyl-H3	Rabbit	1:500	Millipore (#06-599)
H3 total	Rabbit	1:2000	Cell Signaling Technology (#9715)
β-actin	Mouse	1:5000	Sigma (#A5316)
Phospho-Tau (Ser416)	Rabbit	1:1000	Cell signalling (#15013T)
Nrf2	Rabbit	1:500	Abcam (#ab31163)

Secondary antibodies			
Anti-Rabbit (H+L), Alkaline Phosphatase conjugated	Goat	1:10000	Pierce Thermo Fisher Scientific (#31340)
Anti-Mouse (H+L), Alkaline Phosphatase conjugated	Goat	1:10000	Pierce Thermo Fisher Scientific (#31320)

Table 4- Antibodies used for Immunohistochemistry analyses.

Primary antibodies	Host	Dilution	Reference
6E10	Mouse	1:2000	Covance (New Jersey, USA)
AT-8	Mouse	1:2000	Pierce (#MN1020)
Aβ42	Mouse	1:1000	Chemicon Millipore Merck
APP	Rabbit	1:1000	Abcam (Cambridge, UK)
Secondary antibody			
Universal antibody	Horse	1:200	Vectastain Elite ABC kit, Vector Laboratories
Alexa Fluor 594®	Goat	1:1000	Molecular Probes - Invitrogen (Eugene, OR, USA)
Alexa Fluor 488®	Goat	1:1000	Molecular Probes - Invitrogen (Eugene, OR, USA)

3.2 Methods

3.2.1 Animals

Research was conducted in compliance with EU and Portuguese directives regarding the use of laboratory animals (EU Directive 2010/63/EU and Portuguese law DL113/2013, August 7th). All procedures were approved by the local Animal Welfare Committee of the Center for Neuroscience and Cell Biology and Faculty of Medicine, University of Coimbra (ORBEA) and the Portuguese National Authority for Animal Health (DGAV) (ethical permit #211). Animals were housed at our local animal facilities (conventional animal facilities of the Center for Neuroscience and Cell Biology and Faculty of Medicine, University of Coimbra, Coimbra, Portugal), in groups of 3-4 mice per static microisolator cage with a filter

top, and bedding and nesting materials, under controlled temperature (22 º C), humidity (45-65 %) and light conditions (12 h day/night cycle, with lights on at 6 a.m.). Standard hard pellets chow and sterilized and acidified water (pH 2.5-3) were available *ad libitum* throughout the experiment. Signs of distress were carefully monitored and all efforts were made to minimize animal suffering and to reduce the number of animals used. Although not expected, a rapid decrease of body weight (>15-20%) was considered as a humane endpoint for the study.

3.2.2 Genotyping

3xTg-AD and wild-type (WT) mice were genotyped using a DNA polymerase chain reaction (PCR) standard procedure with DNA extracted from an ear punch, by using PS1 forward (CAC ACG CAA CTC TGA CAT GCA CAG GC), PS1 reverse (AGG CAG GAA GAT CAC GTG TTC AAG TAC), APP forward (GCT TGC ACC AGT TCT GGA TGG), APP reverse (GAG GTA TTC AGT CAT GTG CT), Tau forward (GAG GTA TTC AGT CAT GTG CT) and Tau reverse (TTC AAA GTT CAC CTG ATA GT) primers. For the PS1 gene, the PCR protocol consisted of 35 cycles of denaturation - 94 ºC for 40 s; annealing - 62 °C for 40 s and elongation - 72 °C for 1 min. For the APP gene, the PCR protocol consisted of 20 cycles of denaturation – 94 ºC for 30 s; annealing – 53 ºC for 30 s and elongation – 72 ºC for 1 min. For the Tau gene, the PCR protocol consisted of 25 cycles of denaturation – 94 ºC for 30 s; annealing – 52 ºC for 30 s and elongation – 72 ºC for 3 min. PCR products were analysed on 1.7 % agarose gels followed by staining with GreenSafe (NZYtech, Lisboa, Portugal) at 150 V for 30 min with Tris-acetate-EDTA running buffer and visualized under a UV transilluminator (Gel Doc XR system BioRad®, Hercules, USA).

Animals of both genders were subjected to genotyping analysis, but we only use male mice in our studies. Genotypic analysis indicates the presence of human APP (**Figure 12A**), Tau (**Figure 12B**), and PS1 (**Figure 12C**) transgenes in the 3xTg-AD compared to WT mice.
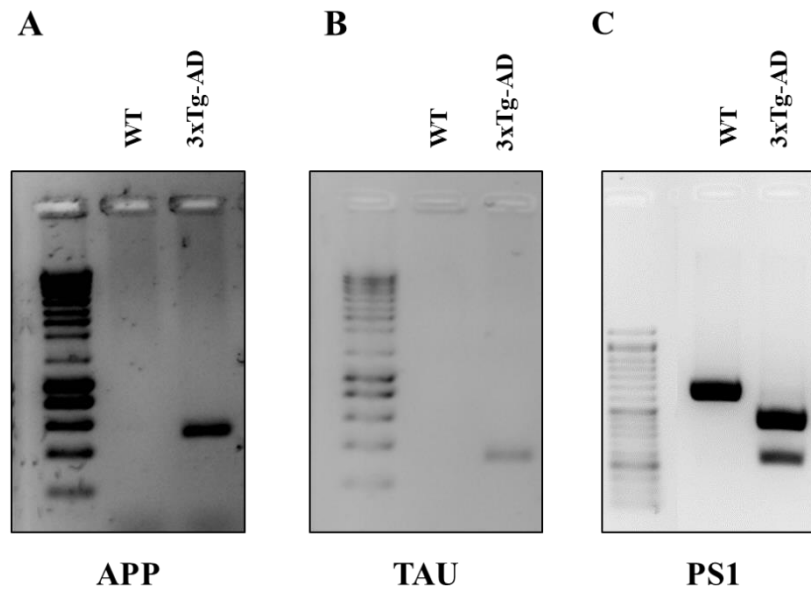
Figure 12- Characterization of experimental animals by genotyping analysis. Representative genotyping data of ear tissue from WT and 3xTg-AD mice male. These results show the presence of APP gene (**A**), TAU gene (**B**) and PS1 (**C**) human genes in 3xTg-AD compared to WT mice.

3.2.3 Mouse mini-osmotic pump implantation surgery and treatment

Twenty-eight 3xTg-AD male mice and twelve age-matched WT male mice were subjected to the subcutaneous implantation of Alzet mini osmotic pumps (model 2006), previously filled with either sterile saline (0.9 % NaCl) or sodium butyrate (SB: 1 mg/kg/day, diluted in sterile saline solution) and primed in sterile saline at 37 ºC for at least 72 h before implantation, according to manufacturer's instructions. Prior to the surgery, mice were submitted to analgesia with subcutaneous buprenorphine (0.10 mg/kg) injection for thirty minutes (starting at 6:30 a.m.), followed by anesthesia with continuous isofluorane inhalation (4-5 % during the induction of sedation and then 1.5-2 % for maintenance) during the overall surgical procedure. Then, a small incision was made in the skin between the scapulae and, with the aid of a hemostat, a small pocket was formed by spreading apart the subcutaneous connective tissues to insert the mini osmotic pump subcutaneously, with the flow moderator pointing away from the incision. The skin incision was then closed with surgical clips. After recovery from anaesthesia, mice were returned to their cage, provided with wet food and water, carefully monitored and administered with post-surgical buprenorphine analgesia (0.05 mg/kg) every 6 h, for at least 24 h. According to the

manufacturer, the content of the mini osmotic pumps was continuously delivered at a flow rate of 0.15 µL/hour, for 42 days. Body weight was measured before, during (once a week) and after treatment.

3.2.4 Behavioural analyses

From the 39th until the 42nd day of treatment, mice transferred to the behavior room on the day before the beginning of behavioral tests to be accustomed to its environment, where they were subjected to several behavioural tests to evaluate their exploratory activity, anxiety and short-term spatial memory. Behavioural tests were performed every day between 7:00 a.m. and 12:00 p.m., for 4 consecutive days, in a silent room, under dim light and with the aid of an experienced observer blind to the experimental conditions. Tests were performed in the following order: Y-maze, open field (OF), object displacement (OD) and novel object recognition (NOR) tests. During this period, mice were maintained in standard housing conditions. Of note, for every behavioral test, the platform was always cleaned with 10 % ethanol between each animal housed in the same cage and 70 % ethanol between animals of different cages. All experiments were continuously recorded by the computer-operated video ANY-MAZE video tracking system and respective software (Stoelting Co., Wood Dale, IL, USA).

3.2.4.1 Modified Y-maze test

The **modified Y-maze** test is a short-term recognition spatial memory test, based on the innate preference of animals to explore areas that have not been previously explored (Soares et al., 2013). It was performed in a Y-shaped plexiglass apparatus consisting of three identical arms (35 cm long, 5 cm wide and 10 cm high), separated by angles of 120º: the Start arm, whereby the animal is placed at the start of the experiment and is always opened; the Other arm, that is opposite to the start arm and also always open; and the Novel arm, that is blocked during the training phase, being opened only during the test phase. During the training session, the mice were allowed to freely explore the Start and the Other arm for 8 min, whereas the Novel arm was blocked (Dellu et al., 1992, 1997; Akwa et al., 2002). After a 120-min inter-trial interval, animals were subjected to the test session, after the removal of the wall that blocked the Novel arm and its opening for free exploration of the three arms

for 8 min (**Figure 13**). Memory performance was given by the percentage of time spent in the novel arm over the time spent exploring all arms.
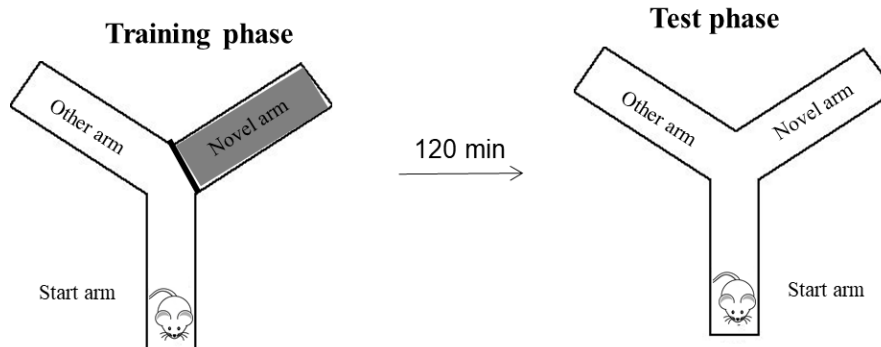
Figure 13- Schematic representation of the modified Y-maze behavioural test. The training phase lasted for 8 min and the mice were allowed to freely explore the Start and Other arm of the maze. After a 120 min inter-trial interval, animals were allowed to explore all three arms for further 8 min.

3.2.4.2. Open field test

The **Open field** behavior test allows the assessment of the locomotor and behavioral activity (namely anxiety-like behavior) in rodents (Gould et al., 2009). Motor activity was evaluated in an open field squared arena with grey open-topped boxes (38 cm wide ×38 cm), using the Stoelting ANY-MAZE video tracking system and respective software to detect the position of the animal's head (**Figure 14**). Mice were placed individually at the corner of the open field arena and allowed to move freely for 10 min. Their exploratory activity within the center and peripheral areas was tracked, and data was calculated by the Any-Maze software.
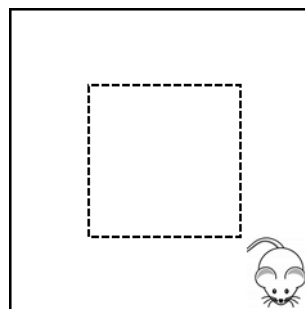
Figure 14- Schematic representation of the open field arena. Animals are allowed to move freely in the arena for 10 min, and their behaviour was monitored. The inner square represents the center of the arena.

3.2.4.3. Object displacement test

The apparatus used for the **Object Displacement** test consisted of a plexiglass dark grey square arena measuring 38×38 cm. During the first 10 min, mice were allowed to move freely in the arena for habituation. Then, during the acquisition phase the animals were allowed to freely explore two identical tall soda cans placed within the arena for further 10 min. These objects were heavy and big enough to prevent mice from moving or climbing them during the trial sessions. After a 90-min inter-trial interval, one of the objects was moved to the opposite place in the arena and mice were allowed to freely explore the objects for other 5 min (test session) (**Figure 15**). Data regarding their exploratory activity was tracked and calculated by the Any-Maze software and presented as $\frac{\text{Time spent exploring the displaced object}}{\text{Time spent exploring the displaced object} + \text{Time spent exploring the non-displaced object}} \times 100$.
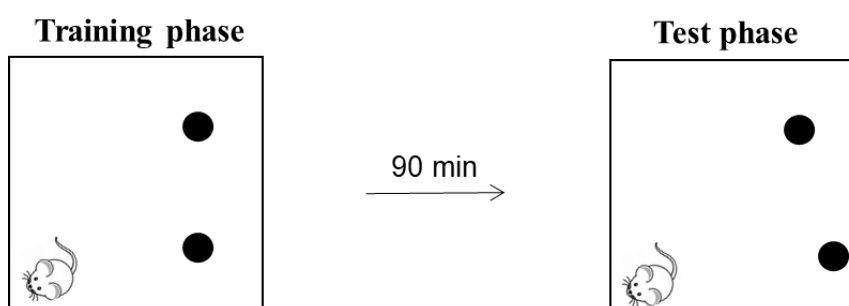
Figure 15- Schematic representation of the object displacement behavioural test. The habituation phase lasted 10 min, during which the mice were allowed to freely explore and become familiar to the arena. Then, during the training phase mice were allowed to freely explore the arena containing two identical tall soda cans for further 10 min. After a 90 min inter-trial interval, one of the objects was moved to its opposite place in the arena and animals were allowed to freely explore the objects for plus 5 min (test phase).

3.2.4.4. Novel object recognition test

The apparatus used for the **Novel Object Recognition** consisted of a dark grey square arena measuring 38×38 cm (**Figure 16**). During the first 10 min, mice were allowed to move freely in the arena for habituation. Then, during the acquisition phase the animals were allowed to freely explore two identical tall soda cans placed within the arena for plus 10 min. These objects were heavy and big enough to prevent the animals from moving or climbing them during the trial sessions. After a 90-min inter-trial interval, one of the cans was replaced by a novel object (a plastic ketchup bottle), but kept in the same position, and the animals were allowed to freely explore the objects for further 5 min. Data regarding their

exploratory activity was tracked and calculated by the Any-Maze software and presented as

$$\frac{\text{Time spent exploring the novel object}}{\text{Time spent exploring the novel object} + \text{Time spent exploring the familiar object}} \times 100.$$
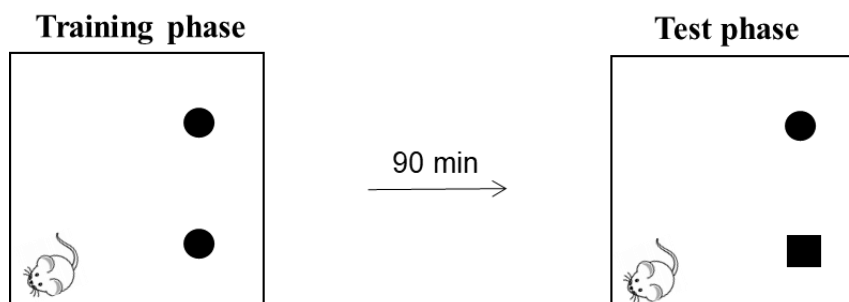

Figure 16- Schematic representation of the novel object recognition behavioural test. The habituation phase lasted 10 min, during which the mice were allowed to freely explore and become familiar to the arena. Then, during the training phase mice allowed to freely explore the arena containing two equal objects for plus 10 min. After a 90 min inter-trial interval, one of the object was replaced by a novel one (plastic ketchup bottle) placed in the same position and the animals allowed to freely explore the objects for plus 5 min (test phase).

3.2.5 Brain tissue preparation for immunohistochemical analysis

Mice were deeply anesthetized with sodium pentobarbital (70 mg/kg i.p.) and perfused transcardially with 0.9 % NaCl, for 14 min, followed by perfusion with 4% paraformaldehyde (4% PFA) in phosphate buffered solution (PBS), containing (in mM): 137 NaCl, 2.7 KCl, 1.8 KH_2PO_4, 10 $Na_2HPO_4 \cdot 2H_2O$, pH 7.4), for further 30 min. The brain was removed and post-fixed in a glass vial with 4 % PFA in PBS for further 24 h, at 4 ℃. Then, fixed brains were rinsed twice with PBS and cryoprotected by immersion in 20 % (w/v) sucrose prepared in PBS, at 4 ℃, until it sank in the bottom of the vial. The brain was then snap frozen in liquid nitrogen and kept at -80 ℃ until cryostat sectioning.

3.2.6 Preparation of protein extracts from brain homogenates

Animals were euthanized by cervical displacement, the brains were collected, the cortex, hippocampus and cerebellum immediately dissected on ice (~4°C) and kept at -80°C until further use for homogenization and preparation of total protein extracts. For these, the previously dissected tissues were homogenized with RIPA lysis buffer (composed by 150 mM NaCl, 50 mM Tris, 5 mM EGTA, 1% Triton X-100, 0.5% deoxycholate, 0.1% sodium dodecylsulphate (SDS), pH 7.5), supplemented with 1 mM dithiotreitol (DTT), 1 mM phenylmethylsulfonyl fluoride (PMSF), plus 1µg/ml protease inhibitor cocktail (containing chymostatin, pepstatin A, leupeptin and antipain), 100 nM okadaic acid, 25 mM sodium

fluoride (NaF), 1 mM sodium orthovanadate (Na$_3$VO$_4$) and 1 µM Trichostatin A (TSA) (a HDACi). The extracts were centrifuged at 3000 *xg*, in an Eppendorf 5417R centrifuge*,* for 15 min, at 4 ºC. The obtained pellet was discarded, and the protein concentration of the supernatant was determined using the Bio-Rad protein assay, following the manufacturer's instructions. Extracts were stored at -20 °C until further use.

3.2.7 Western blotting

Equivalent amounts of protein extracts (10-30 µg) were denatured with 6x concentrated loading buffer (containing 300 mM Tris-HCl (pH 6.8), 12 % SDS, 30 % glycerol, 600 mM DTT, 0.06 % bromophenol blue), at 70 °C, for 10 min, and 20-30 µL of each were loaded and separated by SDS-PAGE (7-15 %). Then, proteins were electrophoresed onto polyvinylidene difluoride (PVDF) membranes. The membranes were blocked with 5 % (w/v) BSA in Tris buffered saline (containing 25 mM Tris-HCl and NaCl 150 mM, pH 7.6) with 0.1 % Tween-20 (TBS-T), for 1h at room temperature (RT) and then incubated overnight at 4 °C with the primary antibodies. After washing the membranes 3 times in TBS-T for 15 min each, anti-mouse or anti-rabbit secondary antibody conjugated to alkaline phosphatase prepared in 1 % (w/v) BSA in TBS-T were applied for 1 h at RT and excess antibody washed 3 times, 15 min with TBS-T. Immunoreactive bands were visualized by alkaline phosphatase activity after incubation with ECF reagent, visualized using a BioRad ChemiDoc Touch Imaging System (BioRad, Hercules, USA) and quantified using Image Lab analysis software (BioRad). All the primary and secondary antibodies, respective dilutions and commercial references are described in **Table 3.**

3.2.8 Immunohistochemistry analysis

Brains collected for immunohistochemistry studies (as detailed elsewhere) were included in Tissue-Tek optimum cutting temperature (O.C.T.) compound and then sectioned into 40 µm-thick coronal sections using a Leica CM3050S cryostat-microtome. Slices were collected in four series and stored in 48-well plates with sterile 0.1 M PBS, supplemented with 0.05 % (v/v) sodium azide, and stored at 4 °C until further use.

3.2.8.1 DAB immunohistochemistry

For immunostaining, slices were rinsed with PBS at RT for 15 minutes with mild agitation. For colorimetric assays (Belfiore et al., 2019), slices were incubated with phenylhydrazine in 1x PBS (1:1000) for 30 min, at 37 ºC. Slices were then rinsed 3 times, 10 min each, with PBS, and blocked in a blocking solution prepared with 10 % goat serum plus 0.2 % Triton X-100 in PBS, for 1h, at RT. Then, slices were incubated with primary antibodies (previously prepared in blocking solution), overnight, at 4 ºC with mild agitation. Slices were then rinsed again 3 times, 10 min each, with PBS and incubated for 1 h at RT with the universal secondary antibody, prepared in blocking solution. Slices were rinsed 3 times, 10 min each, with PBS and then incubated with avidin–biotin complex (ABC, from Vectastain), for 1 h, at RT. Slices were then rinsed twice for 10 min each with PBS and incubated with diaminobenzidine (DAB) for 2-4 min, at RT. Finally, the slices were rinsed 3 times, 10 min each with PBS, mounted on gelatinized glass slides and allowed to dry for 15 min at 37 ºC. Afterwards, tissue sections were progressively dehydrated in 70 % ethanol for 5 min, followed by 95 % ethanol for 5 min, 100 % ethanol for 5 min and, finally, with xylene for 3 times, 2 min each. As a final step Richard-Allan Scientific Mounting Medium was applied and sections covered with glass coverslips and allowed to dry. Immunostainings were visualized on a Zeiss Axio Imager Z2 microscope (Zeiss) using Plan-Apochromat 5x and 10x/0.8 M27 objectives. All primary and secondary antibodies are described in **Table 4.**

3.2.8.1 Fluorescent immunohistochemistry

For immunostaining, slices were rinsed 3 x 10 min with PBS at RT with mild agitation. The slices were incubated with blocking solution of PBS with 3% BSA and 0.2% Triton X-100 for 1 h at RT. Slices were the rinsed 3 x 10 min with PBS, blocked in a blocking solution of 3% BSA and 0.2% Triton X-100 in PBS, during 1 h at RT and incubated with primary antibodies prepared in blocking solution ON, at 4 ºC with mild agitation. Slices were then rinsed 3 x 10 min with PBS and incubated for 2 h at RT with the secondary antibody and Hoechst 33342 prepared in blocking solution. Slices were rinsed 3 x 10 min with PBS and mounted on gelatinized glass slides with DPX mounting medium and allowed to dry. Immunostainings were visualized on a Zeiss Axio Imager Z2 microscope (Zeiss) using Plan-

Apochromat 5x, 10x and 20x/0.8 M27 objectives. All primary and secondary antibodies are described in **Table 4.**

3.2.9 Statistical analysis

Results were presented as scatter plot with bar, with mean ± standard error of the mean (S.E.M.) of the indicated number of mice/group. Statistical analysis and graphic artwork were obtained using the GraphPad Prism 7.0 software (GraphPad Software, San Diego, CA, USA). After the identification of outliers with the ROUT test and after the Kolmogorov-Smirnov normality test, statistical significance was determined by the Student's t-test for comparison between two cohorts with a Gaussian distribution, by one-way ANOVA test followed by the Sidak post-hoc test for multiple groups with a Gaussian distribution, or by the Kruskal-Wallis test (for a non-Gaussian distribution) followed by Dunn's post-test. A p value <0.05 was considered statistically significant: $*p<0.05$, $**p<0.01$ and $***p<0.001$.

CHAPTER IV- Results

4.1 Analysis of body weight in 3xTg-AD mice

To evaluate if sodium-butyrate (SB) administration affects mouse body weight, this parameter was measured before, during and after treatment with SB. Before implantation of mini osmotic pumps, the 3xTg-AD mice present a small, but statistically significant difference in body weight when compared to WT mice (30.62 ± 0.3019 g, n= 25 for 3xTg-AD vs 29.11 ± 1.136 g, n= 10 for WT; $p^{***} < 0.001$, by the Student's t-test; **Figure 17A**). During the treatment, the animals did not suffer significant weight changes until they were moved to the behavior test room (**Figure 17B**), when they presented a tendency, although not significant, for a decrease in body weight during the time they were subjected to the behavioral tests. In general, the body weight is increased in 3xTg-AD animals before, during and after the treatment.
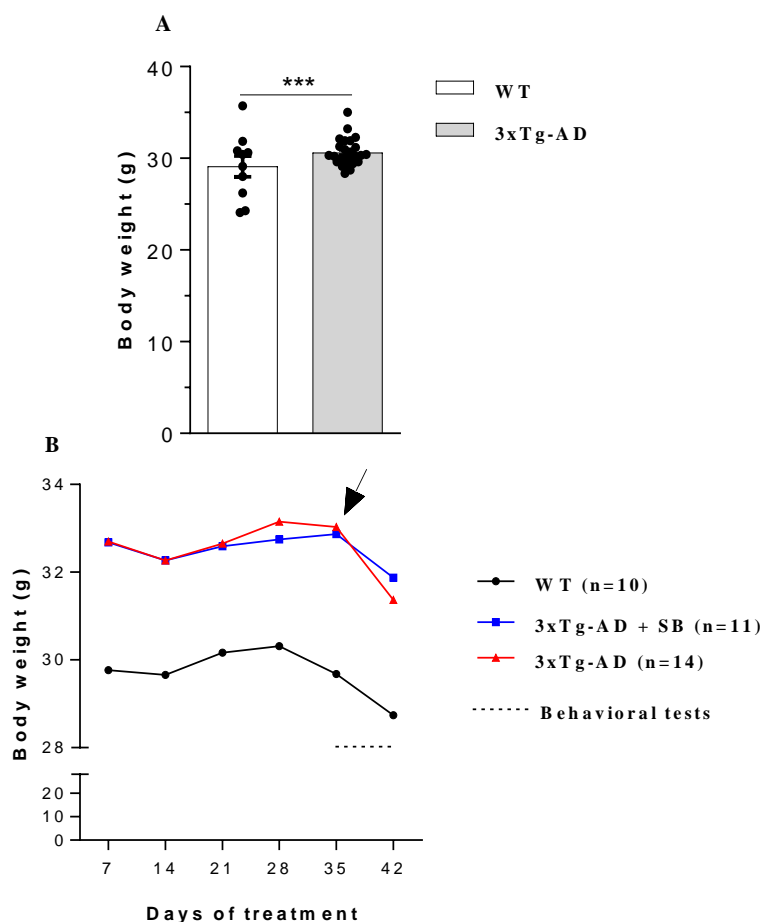
Figure 17- Body weight one day before mini-pumps implantation (A) and during treatment (B). In (**B**), the body weight of animals was measured once a week until the end of treatment with NaCl 0.9% or SB (1mg/kg/day), during 42 days. When indicated (arrow), the animals were moved to behavioral test room for one week, presenting a tendency for a decrease in body weight. Statistical analysis: (**A**) Data are expressed as mean $\pm$ SEM of the number of animals depicted in the graph legend. Statistical analysis: ***$p < 0.001$ vs WT mice (Student's t-test).

4.2 Influence of treatment with sodium butyrate in exploratory activity of 3xTg-AD mice

At day 39 of treatment, the animals were subjected to a variation of the Y-maze test designed to evaluate recognition memory and exploratory activity. 3xTg-AD mice revealed a small tendency, although not significant, for a slight increase in the percentage of entries into the novel arm (41.00 ± 3.11 %, n= 10 for 3xTg-AD vs 35.04 ± 2.93 %, n= 10 for WT; $p= 0.3831$, One way ANOVA with Sidak post-test; **Figure 18A**), in the percent travelled distance in the novel arm (41.39 ± 3.57 %, n= 10 for 3xTg-AD vs 30.59 ± 2.66 %, n= 10 for WT; $p= 0.0869$, One way ANOVA with Sidak post-test; **Figure 18B**) and in the percentage of time spent in the novel arm (39.43 ± 7.63 %, n= 10 for 3xTg-AD vs 34.01 ± 4.88 %, n= 10 for WT; $p= 0.8614$, One way ANOVA with Sidak post-test; **Figure 18C**) compared to WT animals. Treatment of 3xTg-AD mice with SB had no effect on any of these behavioural parameters (39.17 ± 3.44 %, n= 12 for 3xTg-AD+SB vs 41.00 ± 3.11 %, n= 10 for untreated 3xTg-AD, $p= 0.9020$, for the entries into the novel arm; 38.81 ± 3.94 %, n= 12 for 3xTg-AD+SB vs 41.39 ± 3.57 %, n= 10 for untreated 3xTg-AD, $p= 0.8426$ for the distance travelled in the novel arm and 36.94 ± 8.85 %, n= 12 for 3xTg-AD+SB vs 39.43 ± 7.63 %, n= 10 for untreated 3xTg-AD, $p= 0.9661$ for the time spent in the novel arm; One way ANOVA with Sidak post-test for **Figure 18A-C**). SB did not affect recognition memory and exploratory activity in 3xTg-AD mice.
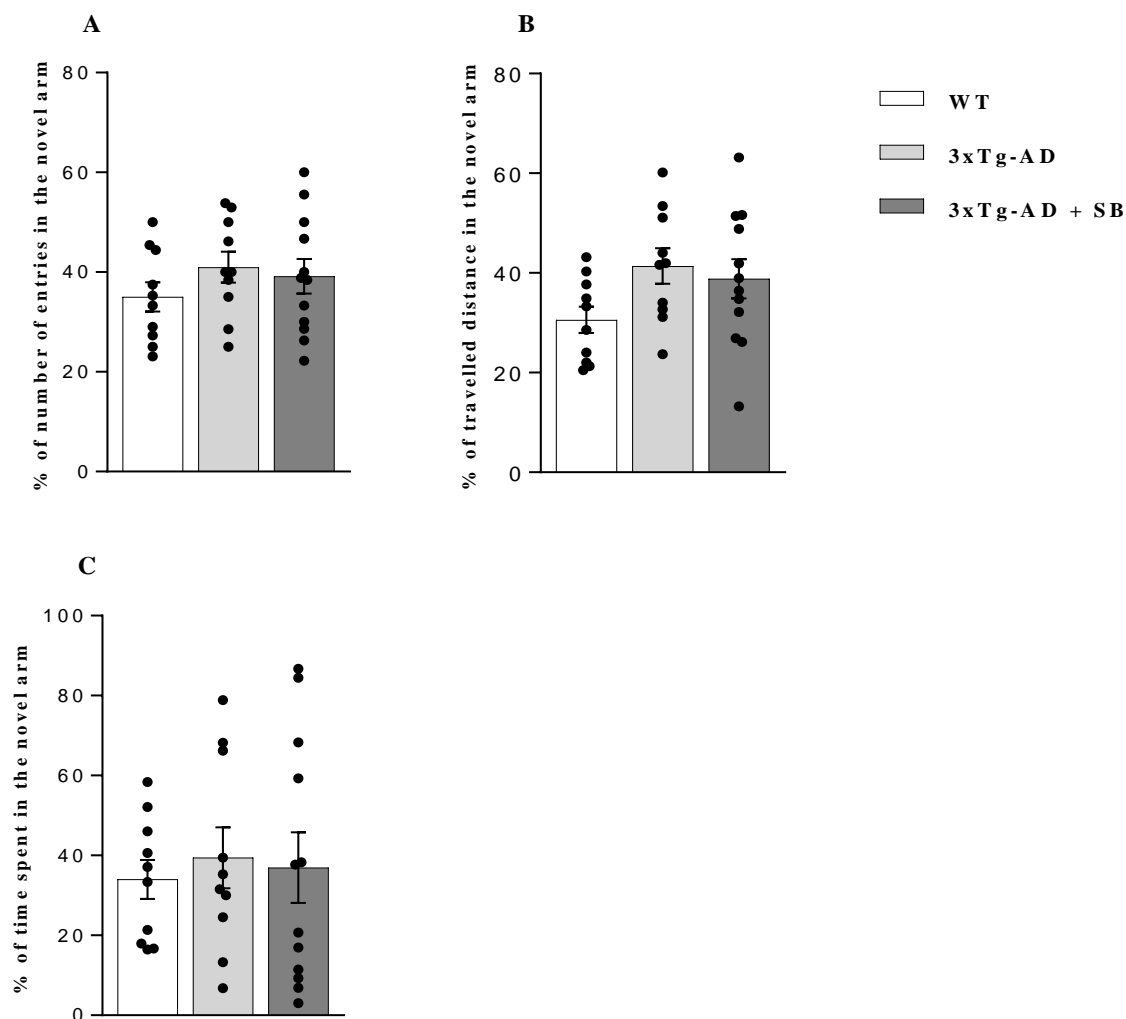
Figure 18- Assessment of exploratory activity and locomotion by Y-maze test in 3xTg-AD mice treated with SB. At the 39th day of treatment, animals performed the Y-maze test. 120 min after the initial training session (that lasted for 8 min), the animals were allowed to explore all three arms (start, other and novel) for 8 min. The percentage of entries (**A**), of travelled distance (**B**) and of time spent (**C**) in the novel arm were evaluated. The data are expressed as mean ± SEM of n=10 WT, n= 10 3xTg-AD and n= 12 3xTg-AD+SB. Statistical analysis was given by the one way-ANOVA test (for a parametric Gaussian distribution), followed by Sidak post-test.

4.3 Effect of sodium butyrate treatment on anxiety-like behaviour in 3xTg-AD mice

At the 40th day of treatment, the animals were subjected to the open field test to evaluate the anxiety-like behavior and locomotor activity. 3xTg-AD mice revealed a tendency for a decrease, although not significant in the time spent in the center of the box when compared to WT mice (23.44 ± 6.47 s, n= 11 for 3xTg-AD vs 52.85 ± 10.59 s , n= 10 for WT; $p= 0.1327$, by the one-way ANOVA for multiple comparisons and a Gaussian distribution, with Sidak post-test; **Figure 19A**) and, therefore, a tendency (again not significant) for an increase in the time spent in the periphery of the arena (573.90 ± 8.50 s, n= 11 for 3xTg-AD vs 542.20 ± 10.59 s , n= 10 for WT; $p= 0.4022$, by the one-way ANOVA for multiple comparisons and a Gaussian distribution, with Sidak post-test; **Figure 19B**), showing a small tendency for increased anxiety like behavior in 3xTg-AD mice. Treatment of these mice with SB clearly increased the time spent in the center of the arena (45.57 ± 12.61 s, n= 13 for 3xTg-AD+SB vs 23.44 ± 6.47 s, n= 11 for untreated 3xTg-AD; $p= 0.02608$, by the one-way ANOVA for multiple comparisons and a Gaussian distribution, with Sidak post-test; **Figure 19A**), and decreased, although not significantly, the time spent in the periphery of the arena (535.50 ± 19.34 s, n= 13 for 3xTg-AD+SB vs 573.90 ± 8.50 s, n= 11 for untreated 3xTg-AD; $p= 0.1326$, by the one-way ANOVA for multiple comparisons and a Gaussian distribution, with Sidak post-test; **Figure 19B**) when compared to untreated 3xTg-AD mice. Furthermore, 3xTg-AD mice travelled a smaller distance than WT mice both in the center (1.041 ± 0.22 m, n= 11 for 3xTg-AD vs 2.03 ± 0.25 m, n= 10 for WT; $p= 0.0217$, by the one-way ANOVA for multiple comparisons and a Gaussian distribution, with Sidak post-test; **Figure 19C**) and in the periphery of the arena (6.84 ± 0.61 m, n= 11 for 3xTg-AD vs 10.60 ± 1.24 m, n= 10 for WT; $p= 0.0109$, by the one-way ANOVA for multiple comparisons and a Gaussian distribution, with Sidak post-test; **Figure 19D**). However, SB treatment had no significant effect on the distance travelled in center (1.19 ± 0.26 m, n= 13 for 3xTg-AD+SB vs 1.04 ± 0.22 m, n= 11 for untreated 3xTg-AD; $p= 0.8825$, by the one-way ANOVA for multiple comparisons and a Gaussian distribution, with Sidak post-test; **Figure 19C**) or in the periphery of the arena (6.59 ± 0.271 m, n= 13 for 3xTg-AD+SB vs 6.84 ± 0.61 m , n= 11 for untreated 3xTg-AD; $p= 0.9711$, by the one-way ANOVA for multiple comparisons and a Gaussian distribution, with Sidak post-test; **Figure 19D**). After the treatment, we conclude that SB has no effect in anxiety-like behaviour in 3xTg-AD mice.
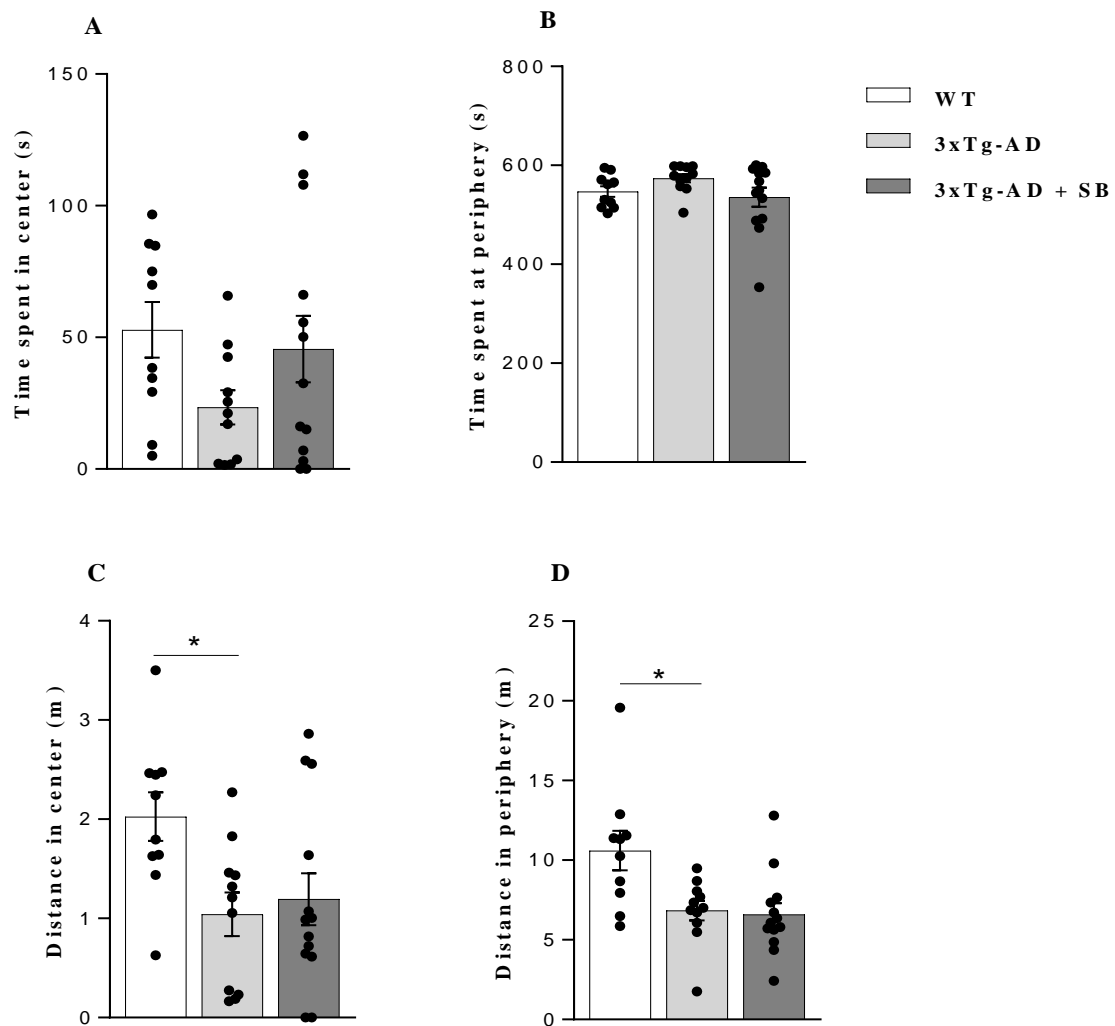
Figure 19- Evaluation of anxiety-like behaviour by the open field test in 3xTg-AD mice following treatment with SB. At the 40th day of treatment, animals performed the open-field test. They were allowed to move freely in the arena of box for 10 minutes. Time spent in center (**A**) and periphery (**B**), and distance travelled in center (**C**) and periphery (**D**) were evaluated. The data are expressed as mean ± SEM of n=10 WT, n= 11 3xTg-AD and n= 13 3xTg-AD+SB. Statistical analysis: *$p < 0.05$ *vs.* saline-treated WT mice, by the one way-ANOVA test (for a parametric Gaussian distribution), followed by Sidak post-test.

### 4.4 Effect of sodium butyrate treatment on spatial memory and recognition in 3xTg-AD mice

At the 41st and 42nd days of treatment, the animals were subjected to the object displacement test to evaluate spatial memory and the novel object recognition to evaluate the recognition capacity, respectively. In the object displacement test, 3xTg-AD animals revealed a small tendency for a decrease in the recognition index (12.93 ± 8.86 %, n= 7 for 3xTg-AD vs 53.59 ± 12.48 %, n= 9 for WT; p= 0.0813, by the Kruskal-Wallis test for multiple comparisons and a non- parametric distribution, with Dunn's post-test, **Figure 20A**) compared to WT animals. Treatment of 3xTg-AD mice with SB revealed a very small tendency for an increase in the recognition index (37.33 ± 13.49 %, n= 11 for 3xTg-AD+SB vs 12.93 ± 8.86 %, n= 7 for untreated 3xTg-AD, p= 0.3427 **Figure 20A**), by the Kruskal-Wallis test for multiple comparisons and a non-parametric distribution, with Dunn's post-test. In the novel object recognition test, we found no differences in performance between 3xTg-AD and WT animals in the recognition index (17.65 ± 17.65 %, n= 5 for 3xTg-AD vs 32.19 ± 16.31 %, n= 6 for WT; p> 0.9999, by the Kruskal-Wallis test for multiple comparisons and a non- parametric distribution, with Dunn's post-test, **Figure 20B**). Furthermore, treatment of 3xTg-AD mice with SB had no effect in the recognition index compared to untreated 3xTg-AD mice (57.07 ± 23.39 %, n= 5 for 3xTg-AD+SB vs 17.65 ± 17.65 %, n= 5 for untreated 3xTg-AD, p= 0.2865, by the Kruskal-Wallis test for multiple comparisons and a non-parametric distribution, with Dunn's post-test, **Figure 20B**). In the both tests, the animals that met the exclusion criteria in the training phase according Vogel-Ciernia and Wood, were excluded from the test phase (Vogel-Ciernia and Wood, 2014). Thus treatment with SB in 3xTg-AD mice had no effect on spatial memory and recognition capacity.
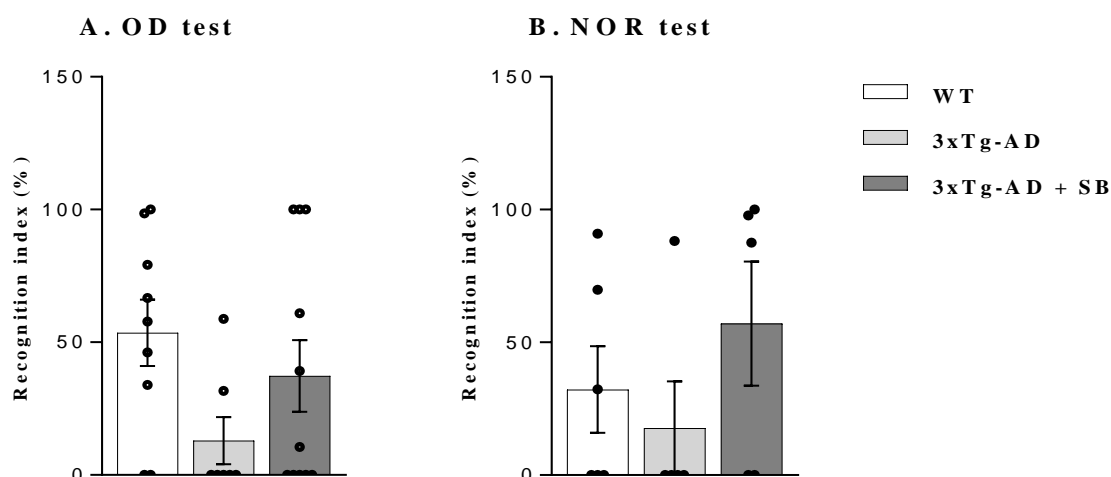
Figure 20- Evaluation of spatial memory (A) by object displacement test and recognition capacity (B) by novel object displacement test in 3xTg-AD mice treated with SB. At the 41st and 42nd days of treatment, animals performed the object displacement (A) and novel object recognition tests (**B**), to assess their spatial and recognition memory capacity. After a 10 min habituation to the open-field arena and the training sessions (10 min), during the test sessions for each behavioural procedure, the animals were allowed to move freely and explore two objects (in OD: one dislocated and one non-dislocated object; in NOR: novel and familiar objects) for 5 minutes. The recognition indexes were calculated as the ratio between the time spent exploring the dislocated/novel object and the total time spent exploring both objects. In OD test we excluded n=1 WT, n= 4 3xTg-AD and n=3 3xTg-AD+SB and n= 4 WT, n= 6 3xTg-AD and n= 9 3xTg-AD+SB for NOR test. The data are expressed as mean ± SEM of n=9 WT, n= 7 3xTg-AD and n= 11 3xTg-AD+SB for OD test and n=6 WT, n= 5 3xTg-AD and n= 5 3xTg-AD+SB for NOR test Statistical analysis was given by the Kruskal-Wallis test (for a non-parametric distribution), followed by Dunn's post-test.

4.5 Influence of sodium butyrate on acetyl H3 levels in 3xTg-AD mice

Considering that SB is a class I HDACi, we further examined the levels of histone acetylation. After the behavioral tests, the animals were euthanized, and total brain cortical extracts were obtained. The levels of acetylated and total histone H3 were evaluated by Western blotting and normalized against beta-actin for each sample. 3xTg-AD mice did not present a significant difference in acetyl H3 levels (0.51 ± 0.23, n= 8 for 3xTg-AD vs 1.00 ± 0.31, n= 8 for WT; $p= 0.2776$, by the Kruskal-Wallis test for multiple comparisons and a non-parametric distribution, with Dunn's post-test **Figure 21A**) or in total H3 levels (1.01 ± 0.27, n= 8 for 3xTg-AD vs 1.00 ± 0.48, n= 8 for WT; $p= 0.9376$, by the Kruskal-Wallis test for multiple comparisons and a non-parametric distribution, with Dunn's post-test **Figure 21B**) compared to WT animals. Treatment of 3xTg-AD mice with SB had no effect on acetyl H3 levels (0.82 ± 0.26, n= 11 for 3xTg-AD+SB vs 0.51 ± 1.10 , n= 8 for untreated 3xTg-AD, $p= 0.6303$, by the Kruskal-Wallis test for multiple comparisons and a non-parametric

distribution, with Dunn's post-test **Figure 21A**) or total H3 levels (1.10 ± 0.24, n= 11 for 3xTg-AD+SB vs 1.01 ± 0.27 , n= 8 for untreated 3xTg-AD, $p > 0.9999$, by the Kruskal-Wallis test for multiple comparisons and a non-parametric distribution, with Dunn's post-test **Figure 21B**) compared to 3xTg-AD mice, either. Therefore, SB had no effect on acetyl H3 levels in 3xTg-AD mice.
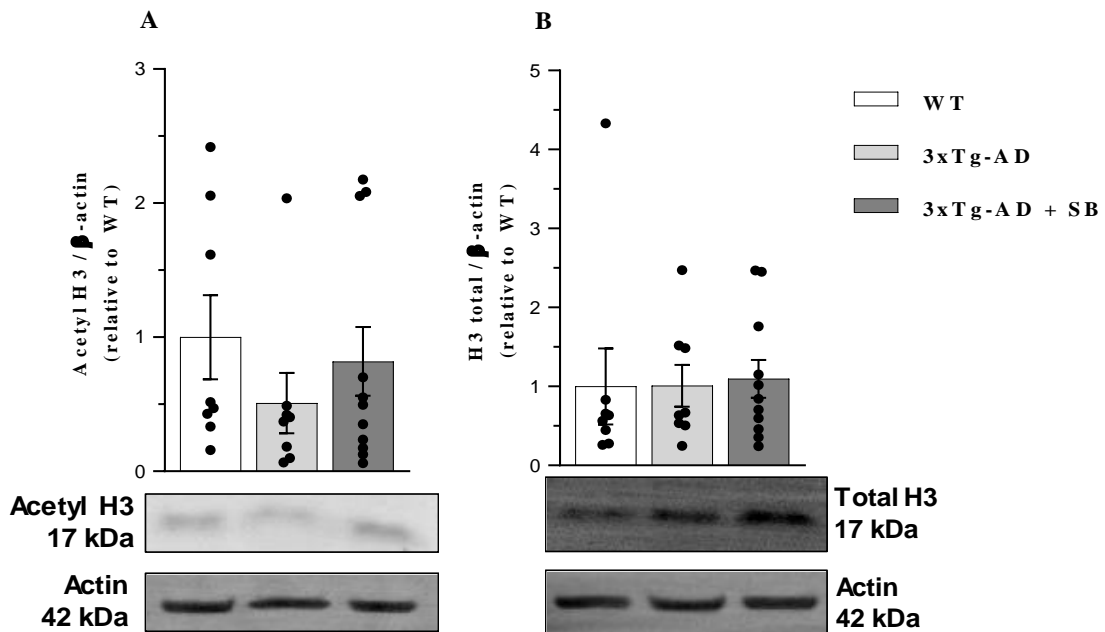
Figure 21- Assessment of histone H3 acetylation in 3xTg-AD mice treated with sodium butyrate. Total brain cortical extracts were obtained by RIPA lysis buffer and probed by Western blotting for acetylated and total H3 levels. Results are expressed as mean ± SEM of band intensities normalized to β-actin levels of n=8 WT, n= 8 3xTg-AD and n= 11 3xTg-AD+SB. Statistical analysis was given by the Kruskal-Wallis test (for a non-parametric distribution), followed by Dunn's post-test.

4.6 Impact of sodium butyrate treatment on pTau and Tau levels in 3xTg-AD mice

The excessive phosphorylation of Tau at Thr231 inhibits the association of Tau to the microtubules (Sengupta et al., 1998) and p(Ser416)Tau, numbered according with the longest isoform of tau, was reported as being one of the main phosphorylation sites *in vitro* (Yamamoto et al., 2005). Considering that a protective therapeutic strategy could impact on AD-related biochemical phenotypes, we also determined Tau phosphorylation at Ser416 and Thr231 residues and total Tau levels by Western blotting in cortical samples of 3xTg-AD mice subjected to SB treatment. 3xTg-AD mice did not present a significant difference in the levels of phosphorylated Tau at Ser416 (1.27 ± 0.27, n= 8 for 3xTg-AD vs 1.00 ± 0.22, n= 8 for WT; $p= 0.7714$, **Figure 22A**), phosphorylated Tau at Thr231 (0.95 ± 0.24, n= 8 for 3xTg-AD vs 1.00 ± 0.22, n= 8 for WT; $p= 0.9866$, **Figure 22B**) or total Tau levels (2.70 ± 0.98, n= 8 for 3xTg-AD vs 1.00 ± 0.44, n= 8 for WT; $p= 0.5406$, **Figure 22C**), when compared to WT animals. Treatment of 3xTg-AD mice with SB had no effect in the levels of phosphorylated Tau at Ser416 (1.45 ± 0.29, n= 11 for 3xTg-AD + SB vs 1.27 ± 0.27, n= 8 for 3xTg-AD; $p= 0.8748$, **Figure 22A**), phosphorylated Tau at Thr231 (0.94 ± 0.21, n= 11 for 3xTg-AD + SB vs 0.95 ± 0.24, n= 8 for 3xTg-AD; $p= 0.9996$, **Figure 22B**) and total Tau levels (3.92 ± 1.43, n= 11 for 3xTg-AD + SB vs 2.70 ± 0.98, n= 8 for 3xTg-AD; $p> 0.9999$, **Figure 22C**) compared to untreated 3xTg-AD mice. One-way ANOVA with Sidak post-test for **Figure 22A, B** and Kruskal-Wallis test for multiple comparisons and a non-parametric distribution, with Dunn's post-test for **Figure 22C**. At the end of the treatment, we concluded that SB had no effect on pTau and Tau levels in 3xTg-AD mice.

A

B

C
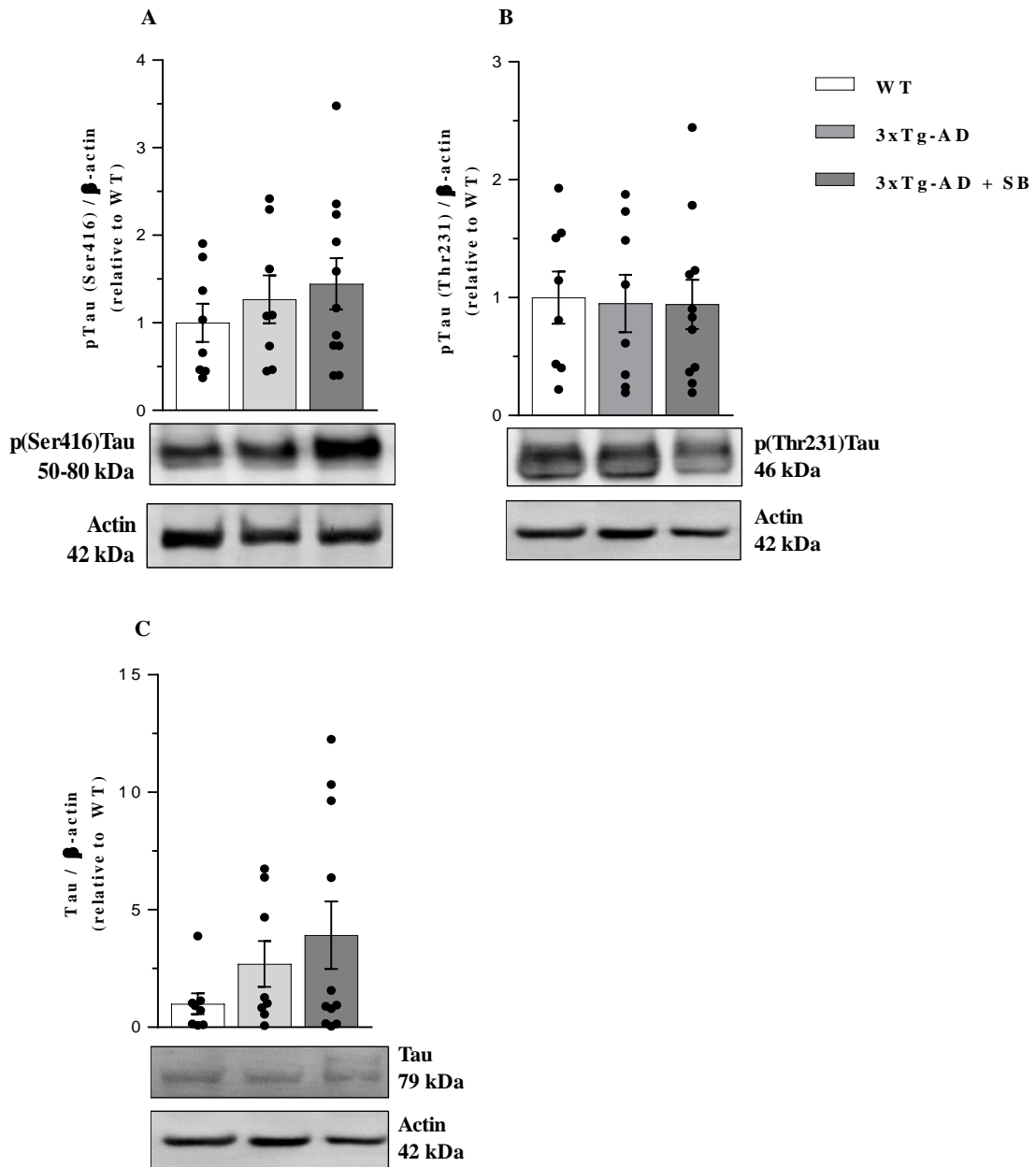
Figure 22- Assessment of Tau phosphorylation and Tau total levels in 3xTg-AD mice treated with SB. Total brain cortical extracts were obtained by RIPA lysis buffer and probed by Western blotting for p(Ser416)Tau, p(Thr231)Tau and total Tau primary antibodies. Results are expressed as mean ± SEM of band intensities normalized to β-actin levels of n=8 WT, n= 8 3xTg-AD and n= 11 3xTg-AD+SB. Statistical analysis was given by the one-way ANOVA test (for a parametric Gaussian distribution), followed by Sidak post-test (**A**), (**B**), and by the Kruskal-Wallis test (for a non-parametric distribution), followed by Dunn's post-test (**C**).

4.7 Analysis of Nrf2 and phosphorylated Nrf2 in 3xTg-AD mice subjected to SB treatment

Because AD pathology has been largely described to account for by increased formation of reactive oxygen species (Schipper et al., 1995) and Nrf2 was previously shown to be altered in the 3xTg-AD model (Mota et al., 2015), we also analyzed the total and phosphorylated levels of Nrf2 at Ser-40 in 3xTg-AD mice treated with SB. This residue is one of the four PKC-mediated phosphorylation sites in human and is critical for a signaling event in a cellular antioxidant response (e.g. Huang et al., 2002).

Nrf2 total levels and p(Ser40)Nrf2 were evaluated by Western blotting after treatment with SB in 3xTg-AD mice and normalized against beta-actin signal for each sample. 3xTg-AD mice did not present a significant difference in Nrf2 levels (1.02 ± 0.07, n= 8 for 3xTg-AD vs 1.00 ± 0.13, n= 8 for WT; $p= 0.9887$, **Figure 23A**) neither pNrf2 levels (1.10 ± 0.23, n= 8 for 3xTg-AD vs 1.00 ± 0.24, n= 8 for WT; $p= 0.9387$, **Figure 23B**) compared to WT animals. Treatment of 3xTg-AD mice with SB had no effect in Nrf2 levels (0.82 ± 0.19, n= 11 for 3xTg-AD + SB vs 1.10 ± 0.23, n= 8 for 3xTg-AD; $p> 0.5807$, **Figure 23A**) nor pNrf2 levels (0.89 ± 0.13, n= 11 for 3xTg-AD + SB vs 1.02 ± 0.07, n= 8 for 3xTg-AD; $p> 0.6679$, **Figure 23B**) compared to 3xTg-AD mice. one-way ANOVA for multiple comparisons and a Gaussian distribution, with Sidak post-test for **Figure 23A, B**. SB had no effect on Nrf2 and pNrf2 levels in 3xTg-AD mice.
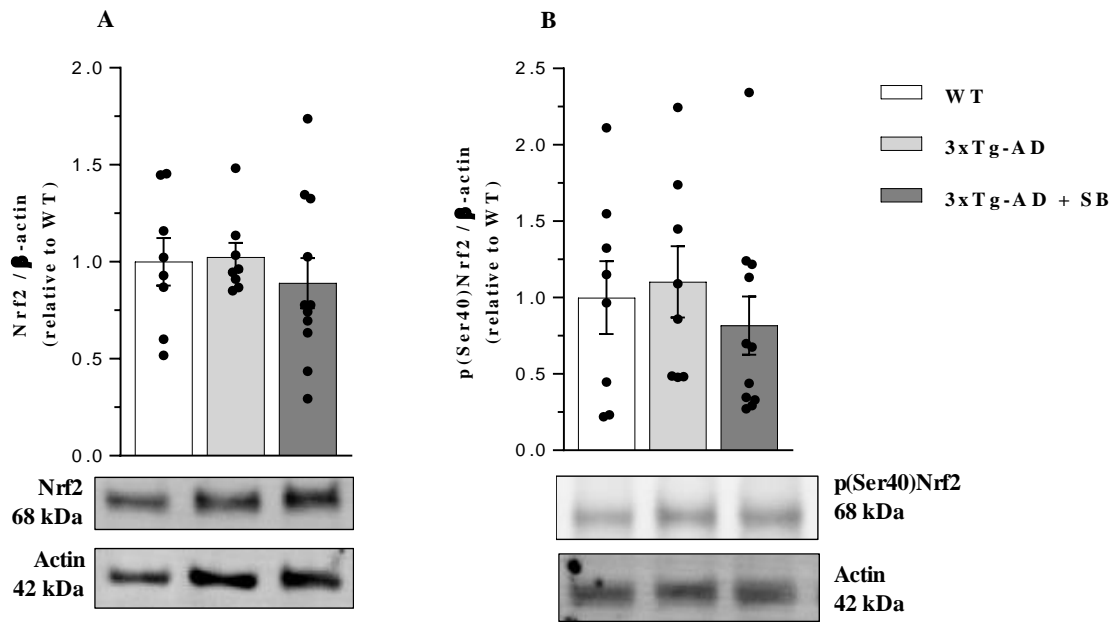
Figure 23- Assessment of total and phosphorylated Nrf2 levels in 3xTg-AD mice treated with SB. Total brain cortical extracts were obtained by RIPA lysis buffer and probed by Western blotting for Nrf2 and p(Ser40)Nrf2 levels. Results are expressed as mean ± SEM of band intensities normalized to β-actin levels of n=8 WT, n= 8 3xTg-AD and n= 11 3xTg-AD+SB. Statistical analysis was given by the one-way ANOVA test (for a parametric Gaussian distribution), followed by Sidak post-test.

4.8 Characterization of neuropathology in 3xTg-AD and WT animals

In order to clarify the histological hallmarks of AD phenotype of 3xTg-AD mice used in this work, Aβ deposition and phosphorylated Tau were examined in brain sections of 3xTg-AD *versus* WT by immunohistochemistry (IHC). Contrary to what was expected, we could not find evidence for intracellular Aβ accumulation (**Figure 24D**) nor extracellular Aβ plaques in the hippocampus of 10.5 months-old 3xTg-AD (**Figure 24B**) or age-matched WT mice (**Figure 24A, C**). Hyperphosphorylated Tau at Ser202 and Thr205 was not present in the hippocampus of 3xTg-AD when compared to age-matched WT mice (**Figure 24E, F**) either.
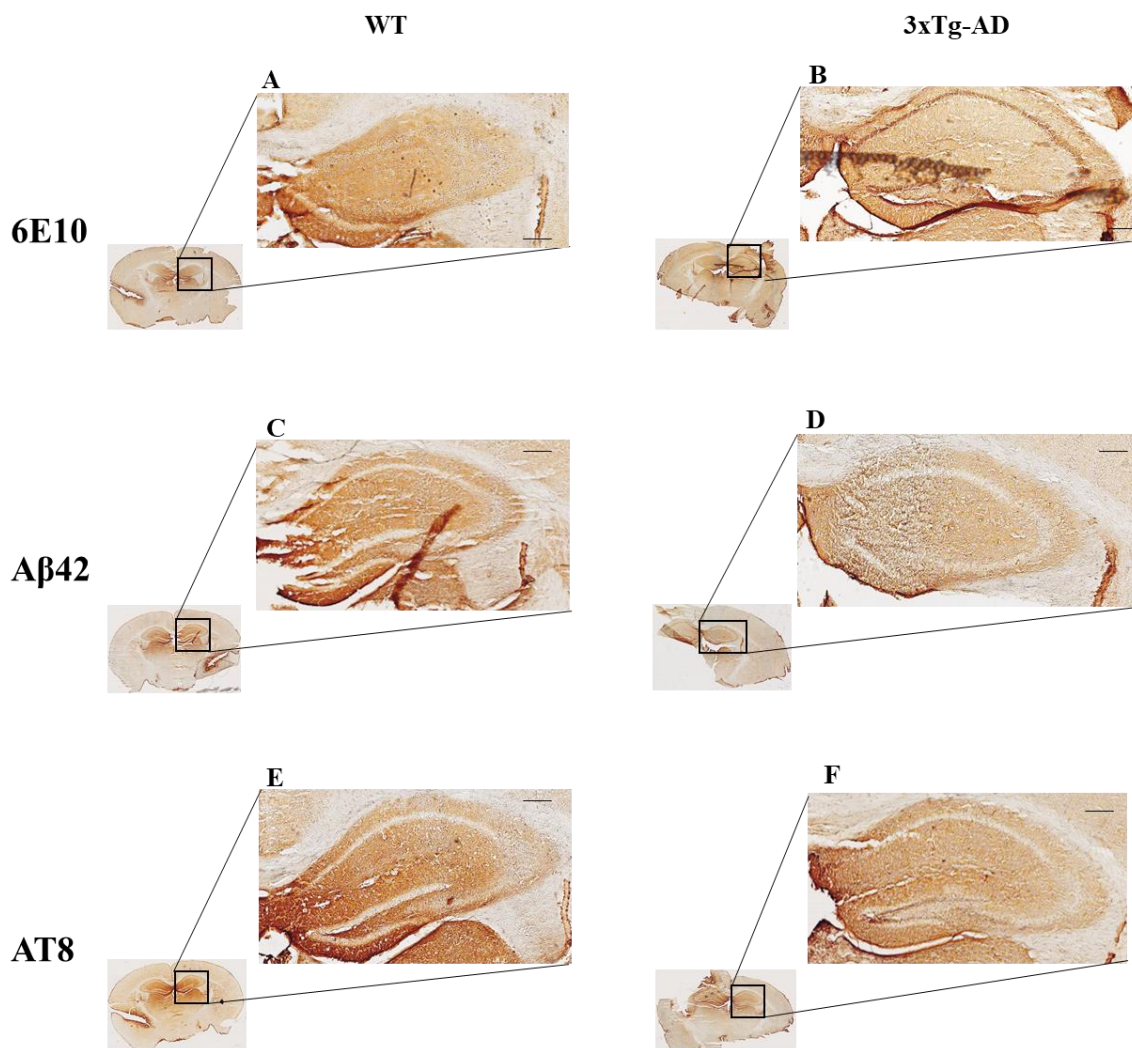
Figure 24- Analysis of Aβ and hyperphosphorylated Tau in 10.5 month-old 3xTg-AD and WT mice. The histological hallmarks of AD phenotype of 3xTg-AD (**B**, **D**, **F**) and WT (**A**, **C**, **E**) mice used in this work were evaluate by IHC. The intracellular Aβ plaques (A, B), extracellular Aβ (C, D) and phosphorylated Tau (E, F) were evaluated in WT and 3xTg-AD mice. Images obtained in Zeiss Axio Imager Z2 microscope (Zeiss) using Plan-Apochromat 5x and 10x/0.8 M27 objectives. Scale bar: 50 μm.

According to Oddo and colleagues, intracellular Aβ appears between 3 and 4 months of age (Oddo et al., 2003). Therefore, we evaluated by fluorescence immunohistochemistry if the 5-month 3xTg-AD animals (**Figure 25A, B**) as well as the animals used in this study (10.5 months) (**Figure 25C, D**) had this characteristic of the disease. As seen previously, no intracellular Aβ presence was observed in the analyzed slices of brain cortex.
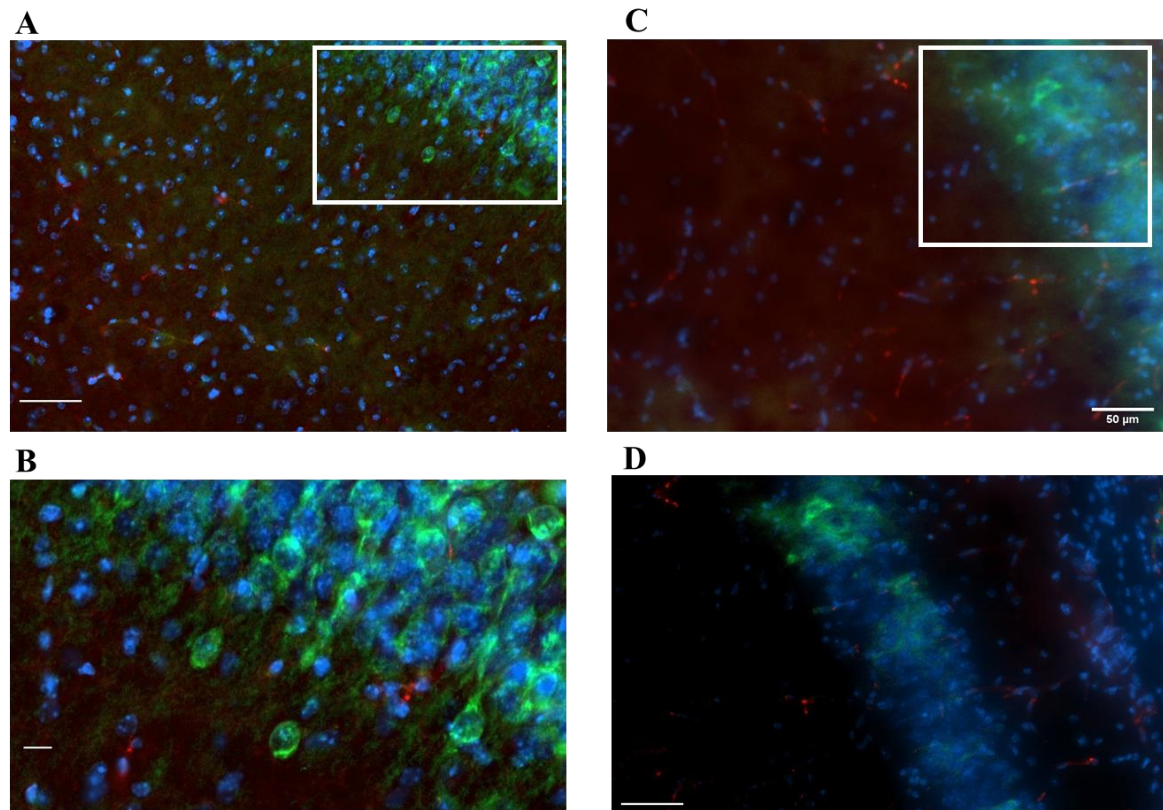
Figure 25- Analysis of intracellular Aβ in 5 and 10.5 months-old 3xTg-AD. The presence of intracellular Aβ plaques (red) were evaluated in slices of brain cortex of 5 months-old (**A, B**) and 10.5 months-old 3xTg-AD mice (**C, D**). Nucleus was visualized by Hoechst staining (blue) and APP was immunostained with a specific antibody (green). Images obtained in Zeiss Axio Imager Z2 microscope (Zeiss) using Plan-Apochromat 5x, 10x and 20x/0.8 M27 objectives. Scale bar: 10 µm for **A** and 50 µm for **B**, **C** and **D**.

CHAPTER V- Discussion

AD is a progressive neurodegenerative disease with no effective treatment. Nevertheless, the study of epigenetic mechanisms is gaining importance to deepen the knowledge of disease factors and pathological mechanisms and, hopefully, to develop efficient treatments (Govindarajan *et al.*, 2011). According to Li and colleagues (Li *et al.*, 2019), histone acetylation plays an important role in learning and memory, by allowing the relaxation of chromatin and subsequent gene transcription. Acetylation levels of histones were altered in AD, most likely due to the increased levels of HDAC in comparison with HATs, thereby decreasing gene transcription (Saha and Pahan, 2006). Indeed, both the sporadic and familial forms of AD were associated with increased DNA compaction and the consequent repression in DNA transcription. Several authors showed that, *e.g.*, the APP/PS1 (Francis *et al.*, 2009) and the Tg2576 mouse models for AD (Ricobaraza *et al.*, 2009) had lower levels of H4 acetylation. Accordingly, others showed that HDACi may constitute a therapeutic strategy against AD, since they allow for the increase in acetylation events. Particularly, HDACis can lower chromatin compaction, thereby increasing gene transcription (*e.g.*, Schneider *et al.*, 2013). These led us to evaluate the effects of peripheral SB (a HDACi) administration in the behavioural and cellular phenotypes of 9 months-old 3xTg-AD mice.

In the present study, 9 months-old 3xTg-AD animals had a significantly larger body weight compared to WT mice, before and during SB treatment. These results are in accordance with previous studies showing that 3xTg-AD mice were heavier than WT animals between the ages of 7 and 12 months (Knight et al., 2013, 2014). In addition, Knight and co-authors revealed that the 3xTg-AD animals have an increased appetite and food consumption (at least until 12 months of age) when compared to WT mice (Knight et al., 2012). According to these authors, until the age of 6 months 3xTg-AD mice did not exhibit significant changes in their metabolic rates, because their larger body mass resulted from a higher food intake, whereas from the age of 7 months onwards, their energetic metabolism becomes altered, with the higher food intake in animals overexpressing Aβ becoming associated with weight loss. This led the authors to hypothesize that, with disease progression upon aging, the 3xTg-AD mice may undergo a hypometabolic state. Our results also showed a tendency for a decrease in body weight among all animal groups after their transfer to the behaviour room. This could be due to: *i)* an increased exploratory activity that,

together with an increased locomotion, could result in a higher energy expenditure; and/or *ii)* an increased anxiety-like behaviour and the subsequent reduction in food intake, thereby accounting for such slight weight loss.

Our study showed no significant effects of treatment with SB on the behavioural tests on memory, learning capacity and anxiety in 3xTg-AD mice. Nevertheless, our observation of increased anxiety-like behaviour in saline-treated 3xTg-AD mice compared to saline-treated WT mice partially agrees with studies showing that the 3xTg-AD mice presented high levels of anxiety between the ages of 7.5 and 11 months, together with difficulties in learning at 6 months of age (Giménez-Llort et al., 2007), weak memory (Stover et al., 2015) and locomotor impairment already in the pre-symptomatic phase (Buchman et al., 2011). In accordance with the behavioural changes described by Sterniczuk and colleagues (Sterniczuk et al., 2010a) in 7.5 to 11 month-old 3xTg-AD female mice, our male saline-treated 3xTg-AD animals also presented higher latency time in the periphery in comparison with age-matched saline-treated WT mice, which spent more time in the center in the open-field arena. This suggests that 3xTg-AD mice may be more anxious than WT ones. Similar observations were reported in 3xTg-AD animals, namely the less time spent in the center of the arena and the lower distance travelled (Filali et al., 2012; Pietropaolo et al., 2014; Pérez-Corredor et al., 2019). Conversely, others reported that 12 month-old 3xTg-AD mice tended to be more hyperactive and slightly more anxious (though not statistically significant) than the WT mice (Pietropaolo et al., 2008, 2014). Hence, anxiety-like behaviour may arise at an initial stage of the disease, possibly before the onset of memory impairment. Even though the anxiety-like phenotype of 3xTg-AD mice was not significantly ameliorated by the peripheral treatment with SB, they tended to present less anxiety-like behaviour (as given by the slight increase in the time spent in the center of the arena and by the slight increment in the distance travelled) in comparison with saline-treated 3xTg-AD mice. Indeed, Govindarajan and co-authors (2011) showed that a 6-week administration of SB (1.2 g/kg/day) to 15 month-old APP/PS1 AD mice at an advanced stage of the disease did not affect their anxiety levels, assessed by the open-field test. More specifically, they observed that the time and distance spent in the center and in the periphery of the arena were similar in APP/PS1 and WT mice. In a more recent study, Cao *et al.* (2018) observed that daily intraperitoneal injection of SB (1.2 g/kg/day) for 21 days did not affect the anxiety levels of

the forebrain presenilin-1 and presenilin-2 conditional double knockout (cDKO) mouse model for AD compared to WT mice. Of note, cDKO mice phenotype was similar to AD patients, and included memory deficits, Tau hyperphosphorylation and cerebral hypertrophy (Cao et al., 2018).

Several studies involving the 3xTg-AD mice did not report significant differences in behavioural tests (like NOR and Morris Water Maze (MWM) tests) before the age of 9 months, eventually with some impairment in short-term memory occurring at 6 month-old (Clinton et al., 2007; Martinez-Coria et al., 2010). Indeed, 6.5 months-old 3xTg-AD mice presented a weak recognition memory, and some locomotor and exploration deficits when compared to WT mice (Stover et al., 2015). At this respect, we did not observe significant differences in the number of entries nor in the time spent in the new arm of the Y-maze apparatus in saline-treated 3xTg-AD mice, though a slight increase in the travelled distance was observed in comparison with WT mice. This is in contrast with a previous report of less entries and time spent in the novel arm of the Y-maze apparatus by 11 month-old 3xTg-AD mice compared to WT mice (Carvalho et al., 2013). Surprisingly, Stover and colleagues found that 6.5 month-old 3xTg-AD mice even performed better than WT animals, which showed less spontaneous alternation (a measure of exploratory and spatial memory), as we also observed in the present study (Stover et al., 2015). This could be explained by the animals' lower interest for novelty. Regarding the object displacement analysis, that aimed to evaluate the effect of SB in the spatial recognition capacity of an object, we observed a tendency towards a higher spatial memory performance in WT mice than in saline-treated 3xTg-AD ones. This appears to be in line with a previous study in 3xTg-AD female mice (Davis *et al*., 2013). Treatment with SB tended to increase the recognition memory performance in 3xTg-AD mice compared with saline-treated 3xTg-AD mice, suggesting a slight improvement in their spatial memory. This is in accordance with the improvement in learning capacity and memory reported in 11 months-old CK-p25 AD mice after daily injections of SB (1.2 g/kg/day) for 4 weeks (Fisher *et al.*, 2007). These mice exhibited progressive neuronal degeneration and death, increased Aβ levels and reduced synaptic plasticity, following p25 overexpression in forebrain neurons (Giusti-Rodríguez et al., 2011). In addition, Cao and co-authors (2018) showed that intraperitoneal treatment with SB for 21 days increases the number of synapses, improving learning and long-term memory in

cDKO mice. In the last behavioural test performed in the present study, we used the novel object recognition test to evaluate the effect of SB treatment on the recognition capacity of 3xTg-AD mice. Our observation that saline-treated 3xTg-AD mice did not present a significant deficit in the object recognition capacity compared to WT mice appears to contradict the previous evidence that the 3xTg-AD mice have deficits in the recognition capacity of objects (Filali et al., 2012). Adding to this, peripheral SB administration did not affect this behavioural trait in 3xTg-AD mice compared with saline-treated AD mice. This may be due to the fact that the animals did not learn the task properly during the training phase and/or did not reveal interest for the new object, as previously reported by Stover et al. (2015) and described above. Following Vogel-Ciernia and colleagues procedure, the mice that remained immobile in the box, or did not explore the two objects and/or presented repetitive movements during the training phase of NOR and OD tests were excluded from the testing phase (Vogel-Ciernia and Wood, 2014). In this behavioural test, the animals might have presented some tiredness, since the number of animals excluded in the last test (NOR) was higher when compared to the number of animals excluded in the OD test.

SB was is a well-known inducer of histone acetylation (Fessler et al., 2013), whose main administration effect includes the increase in acetylation levels of histone H3 (Ferrante et al., 2003; Govindarajan et al., 2011), as described previously. Despite this, we did not find significant differences on brain cortical H3 acetylation levels between 3xTg-AD and WT mice, in contrast with its previously reported reduced levels (Fessler et al., 2013). Since SB is considered a HDACi that crosses the BBB (Liu et al., 2017), its lack of effect on histone acetylation under our experimental conditions was somehow unexpected. This could be due either to a suboptimal dose of SB used here in, to an inefficient drug distribution across the brain cortex and/or to its inefficient ejection from the pump (although the later maybe somehow unlikely, since most SB-treated 3xTg-AD mice displayed H3 acetylation levels in the range of those from saline-treated animals). However, we cannot exclude that SB diffusion across the BBB may have been inefficient, thereby reducing its therapeutic efficacy. This may explain the lack of SB effect on behavioural tests.

Tau phosphorylation levels are often higher in brains from AD patients than in normal individuals (*e.g.*, Li et al., 2019). Evidence point towards 40 potential sites for Tau protein phosphorylation in AD brains, including the Ser416 and Thr231 residues (Lin et al.,

2013; Kimura et al., 2018). For instance, Green *et al*. (2008) showed an increased phosphorylation of Tau protein at Thr231 residue in the brains from 3xTg-AD mice, while more recently others reported that its excessive phosphorylation at this blunts its binding to the microtubules, damages cytoskeletal structure and function and, ultimately, the overall cellular structure (Li et al., 2019). However, in the present study we observed that brain cortical phosphorylation of Tau protein at Thr231 residue was similar in saline-treated 3xTg-AD and WT mice. Adding to this, and in spite of constituting one of the main Tau protein phosphorylation sites *in vitro* (Yamamoto et al., 2005), no significant changes were found in brain cortical levels of Tau protein phosphorylation at the Ser416 residue (these are numbered according to the longest isoform of Tau protein) in 6 month-old 3xTg-AD *versus* WT mice (Gondard *et al.*, 2019). Accordingly, we found that Tau protein phosphorylation at Ser416 was similar in 10.5 month-old, saline-treated 3xTg-AD and WT animals. Our results although demonstrate no effects of peripheral SB treatment on brain cortical Tau protein phosphorylation at Ser416 nor at Thr231 in 3xTg-AD animals. This was somehow unexpected, since Green *et al*. (2008) described that nicotinamide (an inhibitor of class III NAD^{+}-dependent HDACs or sirtuins) administration in drinking water for 4 months to 4 month-old 3xTg-AD mice diminished their levels of Tau protein phosphorylation at Thr231 in comparison with untreated AD mice. However, the authors proposed that these changes were not directly related with transcription regulation, but rather with a nicotinamide-mediated rescue in the Aβ oligomer-associated changes in Tau protein accumulation and degradation mechanisms (Tseng et al., 2008; Green et al., 2008). More specifically, nicotinamide may exert pleiotropic effects towards cytoskeleton, including the removal of Tau protein phosphorylation at Thr231 residue and subsequent tubulin acetylation that may ultimately reinforce microtubule stability (Green *et al.*, 2008). Thus, this increased acetylation of tubulin (or eventually other post-translational modifications) may indirectly contribute for the lower Tau protein phosphorylation in AD, possibly by shifting the later towards microtubule stabilization and maintenance of cellular structure (Li et al., 2019). These data appear to agree with the decrease in hippocampal total phospho Tau protein levels found in AD Tg2576 mice intraperitoneally-administered with 4-PBA (200 mg/kg), another HDACi, between the ages of 7 and 12 months (Ricobaraza et al., 2009). Surprisingly, we did not observe significant differences in total Tau protein levels in the brains from 3xTg-

AD mice, neither after saline nor after SB administration, in contrast with other authors (Walls et al., 2014).

Nrf2 is an active transcription factor under oxidative stress that was decreased in AD brains (Bahn and Jo, 2019). Recent studies showed that SB treatment stimulates the expression of Nrf2 and its target genes (namely HO-1 and NQO1) (Dong et al., 2017). Therefore, we aimed to evaluate the effect of SB treatment on brain Nrf2 levels in 3xTg-AD mice. We observed that brain cortical Nrf2 levels were similar between saline-treated WT and 3xTg-AD mice and that peripheral delivery of SB did not affect its total levels in 3xTg-AD animals. This was somehow unexpected, since SB was recently shown to increase Nrf2 expression in an animal model of diabetic nephropathy (Dong et al., 2017). In addition, no differences occurred in Nrf2 phosphorylation at Ser40 residue between saline-treated 3xTg-AD and WT mice, in contrast with a previous study from our laboratory showing that 3 month-old 3x-Tg-AD mice had higher brain cortical levels of phosphorylated Nrf2 at Ser40 residue (Mota et al., 2015). In line with the above-mentioned maintenance of total Nrf2 levels in 3xTg-AD mice, treatment with SB did not affect its phosphorylation at Ser40 residue either. Since the Nrf2 pathway regulates the expression of antioxidant enzymes with different roles in the brain that depend the disease stage, cell type or its surrounding environment, we anticipate that the evaluation of Nrf2 in nucleic fractions, of its transcriptional activity and/or of the mRNA levels its target antioxidant and detoxifying proteins/enzymes would provide further insights herein.

The 3xTg-AD animal model was created in 2003 by LaFerla's group and has been widely used to study AD pathophysiology. Unfortunately, recent data demonstrate that the latest generations of this transgenic line present initial and progression pathological features that clearly differ from the one initially described ones. Therefore, controversy exists nowadays regarding the use of the 3xTg-AD mice to model AD itself and, in particular, to the evaluate potential therapeutic strategies against its sporadic form (the vast majority of AD cases) (Belfiore et al., 2019). This is further supported by recent studies showing that Aβ plaques and hyperphosphorylated Tau protein deposition occur later than originally described by Oddo and collaborators (2003). Among them, Oddo and colleagues showed in 2018 that 3xTg-AD female mice presented a spectrum of AD phenotypes at later ages than in the original characterization of the colony, including the appearance of an elevated

number of senile plaques only by the age of 12 months, and of neurofibrillary tangle accumulation (containing hyperphosphorylated Tau protein) between the ages of 12 and 20 months. This delay in neuropathology occurs in spite of the higher susceptibility of females to AD (Carroll et al., 2010) and to depression (a condition widely associated with AD), alongside their pre-menopause and subsequent menopause phases starting at 12 to 14 months-old, when their oestrogens and progestogens levels (and protective effects) suddenly drop (Ison and Allen, 2007). Overall, this points towards an even greater delay in the arousal of pathologic AD-like alterations in male 3xTg-AD mice, the only sex cohort used in the present study. To further characterize neuropathologically the WT and 3xTg-AD mice used in our experiments, we performed immunohistochemical analyses of AD-like hallmarks (including intra and extracellular Aβ and hyperphosphorylated Tau protein deposition) in brain tissue from 10.5 months-old animals. As in our previously described results, no significant differences were seen in AD-like neuropathological features in the 3xTg-AD compared to WT mice. This may thus justify the lack of significant behavioural and biochemical differences between the WT and AD mice consistently observed throughout the present work, despite the genotypic confirmation performed at the beginning of the study.

CHAPTER VI- Conclusion

The 3xTg-AD mice were previously shown to present memory, learning and locomotion deficits, and anxiety-like behavior, being histopathologically characterized by the accumulation of Aβ aggregates and hyperphosphorylated Tau protein. Our main objective in the present study was to evaluate the effect of peripheral treatment with SB (an HDACi) as a possible therapeutic strategy against the disease phenotype.

Our behavioral, biochemical and histological results showed that 10.5 months-old, saline-treated 3xTg-AD animals did not manifest most of the expected disease phenotypes. Despite their tendency for an increased anxiety, no memory deficit-related phenotypes were observed, suggesting that a shift of the AD phenotype towards older ages may have occurred. This may ultimately account for our unexpected results with the 3xTg-AD mice that, nonetheless, are in line with the very recent literature. It also reinforces the need for a re-equate its use, especially when evaluating potential therapeutic strategies against sporadic AD. Besides performing similar experiments in another AD transgenic model (such as the APP/PS1 or 5xTg-AD mice), future studies should also include female mice and/or older animals, at a more severe AD stage. Since subcutaneous SB treatment did not increase histone acetylation (another contributor for the lack of differences in our experimental conditions), another possibility is the optimization of dosage, mode of administration and/or treatment duration with SB.

In sum, our results support further studies addressing the role of peripheral HDACi against brain and behavioural changes that arise with AD progression along aging. This will ultimately advance our knowledge on AD pathophysiology and potential therapeutic strategies.

CHAPTER VII-References

Adler P, Mayne J, Walker K, Ning Z, Figeys D (2019) Therapeutic Targeting of Casein Kinase 1δ/ε in an Alzheimer's Disease Mouse Model. bioRxiv Biochem:1–15 Available at: http://biorxiv.org/cgi/content/short/539627v1.

Akwa Y, Ladurelle N, Covey DF, Baulieu E-E (2002) The synthetic enantiomer of pregnenolone sulfate is very active on memory in rats and mice, even more so than its physiological neurosteroid counterpart: Distinct mechanisms? Proc Natl Acad Sci 98:14033–14037.

Alaghband Y, Kwapis JL, López AJ, White AO, Aimiuwu O V., Al-Kachak A, Bodinayake KK, Oparaugo NC, Dang R, Astarabadi M, Matheos DP, Wood MA (2017) Distinct roles for the deacetylase domain of HDAC3 in the hippocampus and medial prefrontal cortex in the formation and extinction of memory. Neurobiol Learn Mem 145:94–104 Available at: http://dx.doi.org/10.1016/j.nlm.2017.09.001.

Albert M, DeKosky S, Dickson D, Dubois B, Feldman H, Fox N, Gamst A, Holtzman D, Agust W, Petersen R, Snyder P, Carrillo M, Thies B, Phelps C (2011) The diagnosis of mild cognitive impairment due to Alzheimer's disease: Recommendations from the National Institute on Aging- Alzheimer's Association workgroups on diagnostic guidelines for Alzheimer's disease. Alzheimer's Dement 7:270–279.

Ansari MA, Scheff SW (2010) Oxidative Stress in the Progression of Alzheimer Disease in the Frontal Cortex. J Neuropathol Exp Neurol 69:155–167.

Armstrong R (2014) A critical analysis of the "amyloid cascade hypothesis". Folia Neuropathol 52:211–225 Available at: http://www.ncbi.nlm.nih.gov/pubmed/25310732.

Bahari-Javan S, Sananbenesi F, Fischer A (2014) Histone-acetylation: A link between Alzheimer's disease and post-traumatic stress disorder? Front Neurosci 8:1–7.

Bahn G, Jo DG (2019) Therapeutic Approaches to Alzheimer's Disease Through Modulation of NRF2. NeuroMolecular Med 21:1–11 Available at: http://dx.doi.org/10.1007/s12017-018-08523-5.

Barage SH, Sonawane KD (2015) Amyloid cascade hypothesis: Pathogenesis and therapeutic strategies in Alzheimer's disease. Neuropeptides 52:1–18 Available at:

http://dx.doi.org/10.1016/j.npep.2015.06.008.

Barucker C, Harmeier A, Weiske J, Fauler B, Albring KF, Prokop S, Hildebrand P, Lurz R, Heppner FL, Huber O, Multhaup G (2014) Nuclear translocation uncovers the amyloid peptide aβ42 as a regulator of gene transcription. J Biol Chem 289:20182–20191.

Bekris L, Yu C-E, Bird T, Tsuang D (2010) Genetics of Alzheimer disease. J Geriatr Psychiatry Neurol 23:213–227.

Belfiore R, Rodin A, Ferreira E, Velazquez R, Branca C, Caccamo A, Oddo S (2019) Temporal and regional progression of Alzheimer's disease-like pathology in 3xTg-AD mice. Aging Cell 18:1–13.

Bordon A (2017) Molecular Mechanisms of Alzheimer's Disease. Sci J Lander Coll Arts Sci 10:5–15.

Buchman AS, Bennett DA, Buchman AS (2011) Loss of motor function in preclinical Alzheimer ' s disease. Expert Rev 11:665–676.

Caldeira GL, Ferreira IL, Rego AC (2013) Impaired Transcription in Alzheimer's Disease: Key Role in Mitochondrial Dysfunction and Oxidative Stress. J Alzheimer's Dis 34:115–131 Available at: http://www.medra.org/servlet/aliasResolver?alias=iospress&doi=10.3233/JAD-121444.

Canning P, Sorrell FJ, Bullock AN (2015) Structural basis of Keap1 interactions with Nrf2. Free Radic Biol Med 88:101–107 Available at: http://dx.doi.org/10.1016/j.freeradbiomed.2015.05.034.

Cao T, Zhou X, Zheng X, Cui Y, Tsien JZ, Li C, Wang H (2018) Histone deacetylase inhibitor alleviates the neurodegenerative phenotypes and histone dysregulation in presenilins-deficient mice. Front Aging Neurosci 10:1–14.

Cao X, Yeo G, Muotri AR, Kuwabara T, Gage FH (2006) Noncoding Rnas in the Mammalian Central Nervous System. Annu Rev Neurosci 29:77–103.

Carroll J, Rosario E, Kreimer S, Villamagna An, Gentzschein E, Stanczyk F, Pike C (2010) Sex differences in β-amyloid accumulation in 3xTg-AD mice: Role of neonatal sex

steroid hormone exposure. Brain Res 17:233–245.

Carvalho C, Machado N, Mota PC, Correia SC, Cardoso S, Santos RX, Santos MS, Oliveira CR, Moreira PI (2013) Type 2 diabetic and alzheimer's disease mice present similar behavioral, cognitive, and vascular anomalies. J Alzheimer's Dis 35:623–635.

Cheignon C, Tomas M, Bonnefont-Rousselot D, Faller P, Hureau C, Collin F (2018) Oxidative stress and the amyloid beta peptide in Alzheimer's disease. Redox Biol 14:450–464 Available at: http://dx.doi.org/10.1016/j.redox.2017.10.014.

Chen GF, Xu TH, Yan Y, Zhou YR, Jiang Y, Melcher K, Xu HE (2017) Amyloid beta: Structure, biology and structure-based therapeutic development. Nature 38:1205–1235 Available at: http://dx.doi.org/10.1038/aps.2017.28.

Chen JH, Lin KP, Chen YC (2009) Risk factors for dementia. J Formos Med Assoc 108:754–764 Available at: http://dx.doi.org/10.1016/S0929-6646(09)60402-2.

Chen S, Ge X, Chen Y, Lv N, Liu Z, Yuan W (2013a) Advances with RNA interference in Alzheimer's disease research. Dovepress 7:117–125.

Chen Y, Liang Z, Blanchard J, Dai CL, Sun S, Lee MH, Grundke-Iqbal I, Iqbal K, Liu F, Gong CX (2013b) A non-transgenic mouse model (icv-STZ mouse) of Alzheimer's disease: similarities to and differences from the transgenic model (3xTg-AD mouse). Mol Neurobiol 47:711–725.

Clinton LK, Billings LM, Green KN, Caccamo A, Ngo J, Oddo S, McGaugh JL, LaFerla FM (2007) Age-dependent sexual dimorphism in cognition and stress response in the 3xTg-AD mice. Neurobiol Dis 28:76–82.

Delcuve GP, Khan DH, Davie JR (2012) Roles of histone deacetylases in epigenetic regulation: Emerging paradigms from studies with inhibitors. Clin Epigenetics 4:1–13 Available at: http://www.clinicalepigeneticsjournal.com/content/4/1/5.

Dellu F, Fauchey V, Le Moal M, Simon H (1997) Extension of a new two-trial memory task in the rat: Influence of environmental context on recognition processes. Neurobiol Learn Mem 67:112–120.

Dellu F, Mayo W, Cherkaoui J, Le Moal M, Simon H (1992) A two-trial memory task with

automated recording: study in young and aged rats. Brain Res 588:132–139.

Dinkova-Kostova AT, Kostov R V., Kazantsev AG (2018) The role of Nrf2 signaling in counteracting neurodegenerative diseases. FEBS J 285:3576–3590.

Dong W, Jia Y, Liu X, Zhang H, Li T, Huang W (2017) Sodium butyrate activates NRF2 to ameliorate diabetic nephropathy possibly via inhibition of HDAC. J Endocrinol 232:71–83.

Dubois B, Feldman HH, Jacova C, DeKosky ST, Barberger-Gateau P, Cummings J, Delacourte A, Galasko D, Gauthier S, Jicha G, Meguro K, O'Brien J, Pasquier F, Robert P, Rossor M, Salloway S, Stern Y, Visser PJ, Scheltens P (2007) Research criteria for the diagnosis of Alzheimer's disease: revising the NINCDS-ADRDA criteria. Lancet Neurol 6:734–746.

Esteras N, Dinkova-Kostova AT, Abramov AY (2016) Nrf2 activation in the treatment of neurodegenerative diseases: a focus on its role in mitochondrial bioenergetics and function. Biol Chem 397:383–400 Available at: http://www.degruyter.com/view/j/bchm.2016.397.issue-5/hsz-2015-0295/hsz-2015-0295.xml.

Fão L, Mota SI, Rego AC (2019) c-Src regulates Nrf2 activity through PKCδ after oxidant stimulus. Biochim Biophys Acta - Mol Cell Res 1866:686–698 Available at: https://doi.org/10.1016/j.bbamcr.2019.01.011.

Ferrante R, Kubilus J, Lee J, Ryu H, Beesen A, Zucker B, Smith K, Kowall N, Ratan R, Luthi-Carter R, Hersch S (2003) Histone deacetylase inhibition by sodium butyrate chemotherapy ameliorates the neurodegenerative phenotype in Huntington's disease mice. J Neurosci 23:9418–9427.

Ferreiro E, Baldeiras I, Ferreira IL, Costa RO, Rego AC, Pereira CF, Oliveira CR (2012) Mitochondrial- and Endoplasmic Reticulum-Associated Oxidative Stress in Alzheimer's Disease: From Pathogenesis to Biomarkers. Int J Cell Biol 2012:1–23.

Fertan E, Rodrigues GJ, Wheeler R V., Goguen D, Wong AA, James H, Stadnyk A, Brown RE, Weaver ICG (2019) Cognitive Decline, Cerebral-Spleen Tryptophan Metabolism, Oxidative Stress, Cytokine Production, and Regulation of the Txnip Gene in a Triple

Transgenic Mouse Model of Alzheimer Disease. Am J Pathol 189:1435–1450 Available at: https://doi.org/10.1016/j.ajpath.2019.03.006.

Fessler E, Chibane F, Wang Z, Chuang D-M (2013) Potential Roles of HDAC Inhibitors in Mitigating Ischemia- induced Brain Damage and Facilitating Endogenous Regeneration and Recovery. Curr Pharmacol 19:5105–5120.

Filali M, Lalonde R, Theriault P, Julien C, Calon F, Planel E (2012) Cognitive and non-cognitive behaviors in the triple transgenic mouse model of Alzheimer's disease expressing mutated APP, PS1, and Mapt (3xTg-AD). Behav Brain Res 234:334–342 Available at: http://dx.doi.org/10.1016/j.bbr.2012.07.004.

Fischer A, Sananbenesi F, Wang X, Dobbin M, Tsai LH (2007) Recovery of learning and memory is associated with chromatin remodelling. Nature 447:178–182.

Francis YI, Fà M, Ashraf H, Zhang H, Staniszewski A, Latchman DS, Arancio O (2009) Dysregulation of histone acetylation in the APP/PS1 mouse model of Alzheimer's disease. J Alzheimer's Dis 18:131–139.

Frost G, Li YM (2017) The role of astrocytes in amyloid production and Alzheimer's disease. Open Biol 7:1–14.

Giménez-Llort L, Blázquez G, Cañete T, Johansson B, Oddo S, Tobeña A, LaFerla FM, Fernández-Teruel A (2007) Modeling behavioral and neuronal symptoms of Alzheimer's disease in mice: A role for intraneuronal amyloid. Neurosci Biobehav Rev 31:125–147.

Giusti-Rodríguez P, Gao J, Graff J, Rei D, Soda T, Tsai L-H (2011) Synaptic deficits are rescued in the p25/Cdk5 model of neurodegeneration by the reduction of β-secretase (BACE1). J Neurosci 31:15751–15756.

Glabe CG (2006) Common mechanisms of amyloid oligomer pathogenesis in degenerative disease. Neurobiol Aging 27:570–575.

González-Reyes RE, Nava-Mesa MO, Vargas-Sánchez K, Ariza-Salamanca D, Mora-Muñoz L (2017) Involvement of Astrocytes in Alzheimer's Disease from a Neuroinflammatory and Oxidative Stress Perspective. Front Mol Neurosci 10:1–20.

Gould TD, Dao DT, Kovacsics CE (2009) Mood and Anxiety Related Phenotypes in Mice. Neuromethods 42 Available at: http://link.springer.com/10.1007/978-1-61779-313-4.

Govindarajan N, Agis-Balboa RC, Walter J, Sananbenesi F, Fischer A (2011) Sodium butyrate improves memory function in an alzheimer's disease mouse model when administered at an advanced stage of disease progression. J Alzheimer's Dis 26:187–197.

Gräff J, Kim D, Dobbin MM, Tsai L-H (2011) Epigenetic Regulation of Gene Expression in Physiological and Pathological Brain Processes. Physiol Rev 91:603–649.

Green KN, Steffan JS, Martinez-Coria H, Sun X, Schreiber SS, Thompson LM, LaFerla FM (2008) Nicotinamide Restores Cognition in Alzheimer's Disease Transgenic Mice via a Mechanism Involving Sirtuin Inhibition and Selective Reduction of Thr231-Phosphotau. J Neurosci 28:11500–11510 Available at: http://www.jneurosci.org/cgi/doi/10.1523/JNEUROSCI.3203-08.2008.

Gu L, Guo Z (2013) Alzheimer's Aβ42 and Aβ40 peptides form interlaced amyloid fibrils. J Neurochem 126:305–311.

Guan JS, Haggarty SJ, Giacometti E, Dannenberg JH, Joseph N, Gao J, Nieland TJF, Zhou Y, Wang X, Mazitschek R, Bradner JE, DePinho RA, Jaenisch R, Tsai LH (2009) HDAC2 negatively regulates memory formation and synaptic plasticity. Nature 459:55–60 Available at: http://dx.doi.org/10.1038/nature07925.

Guerreiro R, Bras J (2015) The age factor in Alzheimer's disease. Genome Med 7:1–3 Available at: http://dx.doi.org/10.1186/s13073-015-0232-5.

Hardy J (2006) A Hundred Years of Alzheimer's Disease Research. Neuron 52:3–13.

Hardy J, Selkoe D (2002) The Amyloid Hypothesis of Alzheimer's Disease. Science (80-) 297:353–357.

Hockly E, Richon VM, Woodman B, Smith DL, Zhou X, Rosa E, Sathasivam K, Ghazi-Noori S, Mahal A, Lowden PAS, Steffan JS, Marsh JL, Thompson LM, Lewis CM, Marks PA, Bates GP (2003) Suberoylanilide hydroxamic acid, a histone deacetylase inhibitor, ameliorates motor deficits in a mouse model of Huntington's disease. Proc Natl Acad Sci 100:2041–2046.

Huang HC, Nguyen T, Pickett CB (2002) Phosphorylation of Nrf2 at Ser-40 by protein kinase C regulates antioxidant response element-mediated transcription. J Biol Chem 277:42769–42774.

Huber CM, Yee C, May T, Dhanala A, Mitchell CS (2018) Cognitive Decline in Preclinical Alzheimer's Disease: Amyloid-Beta versus Tauopathy. J Alzheimer's Dis 61:265–281.

Ison J, Allen P (2007) Pre- but not post-menopausal female CBA/CaJ mice show less prepulse inhibition than male mice of the same age. Behav Brain Res 185:76–81.

Jack Jr C, Knopman D, Jagust W, Shaw L, Aisen P, Weiner M, Petersen R, Trojanowski J (2010) Hypothetical Pathological Cascade in Alheimer's Disease. Lancet Neurol 9:1–20.

Janczura KJ, Volmar C-H, Sartor GC, Rao SJ, Ricciardi NR, Lambert G, Brothers SP, Wahlestedt C (2018) Inhibition of HDAC3 reverses Alzheimer's disease-related pathologies in vitro and in the 3xTg-AD mouse model. Proc Natl Acad Sci 115:11148–11157.

Johnson DA, Johnson JA (2015) Nrf2—a therapeutic target for the treatment of neurodegenerative diseases. Free Radic Biol Med 88:253–267.

Joshi G, Gan KA, Johnson DA, Johnson JA (2015) Increased AD-like pathology in the APP/PS1 E9 mouse model lacking Nrf2 through modulation of autophagy. Neurobiol Aging 36:664–679.

Kanninen K, Malm TM, Jyrkkänen HK, Goldsteins G, Keksa-Goldsteine V, Tanila H, Yamamoto M, Ylä-Herttuala S, Levonen AL, Koistinaho J (2008) Nuclear factor erythroid 2-related factor 2 protects against beta amyloid. Mol Cell Neurosci 39:302–313 Available at: http://dx.doi.org/10.1016/j.mcn.2008.07.010.

Khan M, Ahsan F, Ahmad U, Akhtar J, Badruddeen, Mujahid M (2016) Alzheimer disease: a review. World J Pharm Pharm Sci 5:649–666.

Khemka V, Ganguly A, Chakrabarti S, Banerjee A, Biswas A, Chatterjee G (2015) Metabolic Risk Factors of Sporadic Alzheimer's Disease: Implications in the Pathology, Pathogenesis and Treatment. Aging Dis 6:282–299.

Kilgore M, Miller CA, Fass DM, Hennig KM, Haggarty SJ, Sweatt JD, Rumbaugh G (2010) Inhibitors of class 1 histone deacetylases reverse contextual memory deficits in a mouse model of alzheimer's disease. Neuropsychopharmacology 35:870–880 Available at: http://dx.doi.org/10.1038/npp.2009.197.

Kimura T, Sharma G, Ishiguro K, Hisanaga S (2018) Phospho-Tau Bar Code: Analysis of Phosphoisotypes of Tau and Its Application to Tauopathy. Front Neurosci 12:1–9 Available at: http://journal.frontiersin.org/article/10.3389/fnins.2018.00044/full.

Knight EM, Brown TM, Gumusgoz S, Smith JCM, Waters EJ, Allan SM, Lawrence CB (2013) Age-related changes in core body temperature and activity in triple-transgenic Alzheimer's disease (3xTgAD) mice. Dis Model Mech 6:160–170.

Knight EM, Martins IVA, Gümüsgöz S, Allan SM, Lawrence CB (2014) High-fat diet-induced memory impairment in triple-transgenic Alzheimer's disease (3xTgAD) mice isindependent of changes in amyloid and tau pathology. Neurobiol Aging 35:1821–1832 Available at: http://dx.doi.org/10.1016/j.neurobiolaging.2014.02.010.

Knight EM, Verkhratsky A, Luckman SM, Allan SM, Lawrence CB (2012) Hypermetabolism in a triple-transgenic mouse model of Alzheimer's disease. Neurobiol Aging 33:187–193 Available at: http://dx.doi.org/10.1016/j.neurobiolaging.2010.02.003.

Kocahan S, Doğan Z (2017) Mechanisms of Alzheimer's Disease Pathogenesis and Prevention: The Brain, Neural Pathology, N-methyl-D-aspartate Receptors, Tau Protein and Other Risk Factors. Clin Psychopharmacol Neurosci 15:1–8 Available at: http://www.cpn.or.kr/journal/view.html?doi=10.9758/cpn.2017.15.1.1.

Krishna K, Behnisch T, Sajikumar S (2016) Inhibition of Histone Deacetylase 3 Restores amyloid-β Oligomer-Induced Plasticity Deficit in Hippocampal CA1 Pyramidal Neurons. J Alzheimer's Dis 51:783–791.

Lancet T (2011) The three stages of Alzheimer's disease. Lancet 377:1465 Available at: http://dx.doi.org/10.1016/S0140-6736(11)60582-5.

Levenson JM, O'Riordan KJ, Brown KD, Trinh MA, Molfese DL, Sweatt JD (2004) Regulation of histone acetylation during memory formation in the hippocampus. J Biol

Chem 279:40545–40559.

Li L, Jiang Y, Hu W, Tung YC, Dai C, Chu D, Gong CX, Iqbal K, Liu F (2019) Pathological Alterations of Tau in Alzheimer's Disease and 3xTg-AD Mouse Brains. Mol Neurobiol:1–16.

Li X, Fang P, Mai J, Choi ET, Wang H, Yang XF (2013) Targeting mitochondrial reactive oxygen species as novel therapy for inflammatory diseases and cancers. J Hematol Oncol 6:1–19.

Lin L, Huang QX, Yang SS, Chu J, Wang JZ, Tian Q (2013) Melatonin in Alzheimer's disease. Int J Mol Sci 14:14575–14593.

Liu J, Wang F, Liu S, Du J, Hu X, Xiong J, Fang R, Chen W, Sun J (2017) Sodium butyrate exerts protective effect against Parkinson's disease in mice via stimulation of glucagon like peptide-1. J Neurol Sci 381:176–181 Available at: http://dx.doi.org/10.1016/j.jns.2017.08.3235.

Lovell MA, Xie C, Markesbery WR (1998) Decreased glutathione transferase activity in brain and ventricular fluid in Alzheimer's disease. Neurology 51:1562–1566.

Magalingam KB, Radhakrishnan A, Ping NS, Haleagrahara N (2018) Current Concepts of Neurodegenerative Mechanisms in Alzheimer's Disease. Biomed Res Int 2018:1–12.

Maloney B, Lahiri DK (2011) The Alzheimer's amyloid β-peptide (Aβ) binds a specific DNA Aβ-interacting domain (AβID) in the APP, BACE1, and APOE promoters in a sequence-specific manner: Characterizing a new regulatory motif. Gene 488:1–12 Available at: http://dx.doi.org/10.1016/j.gene.2011.06.004.

Martinez-Coria H, Green KN, Billings LM, Kitazawa M, Albrecht M, Rammes G, Parsons CG, Gupta S, Banerjee P, LaFerla FM (2010) Memantine improves cognition and reduces Alzheimer's-like neuropathology in transgenic mice. Am J Pathol 176:870–880.

Masters C, Bateman R, Blennow K, Rowe C, Sperling R, Cummings J (2015) Alzheimer's disease. Nat Rev 1:1–18 Available at: http://dx.doi.org/10.1038/nrdp.2015.56.

Mayeux R (2004) Biomarkers: Potential Uses and Limitations. Am Soc Exp Neurother Inc

1:182–188.

Mayeux R, Stern Y (2012) Epidemiology of Alzheimer Disease. Cold Spring Harb Perspect Med 7:1–18 Available at: http://www.medscape.org/viewarticle/736977.

McLean C, Cherny R, Fraser F, Fuller S, Smith M, Beyreuther K, Bush A, Masters C (1999) Soluble pool of AB amyloid as a determinant of severity of neurodegeneration in Alzheimer's disease. Ann Neurol 46:860–866 Available at: http://doi.wiley.com/10.1002/1531-8249%28199912%2946%3A6%3C860%3A%3AAID-ANA8%3E3.0.CO%3B2-M.

Mota SI, Costa RO, Ferreira IL, Santana I, Caldeira GL, Padovano C, Fonseca AC, Baldeiras I, Cunha C, Letra L, Oliveira CR, Pereira CMF, Rego AC (2015) Oxidative stress involving changes in Nrf2 and ER stress in early stages of Alzheimer's disease. Biochim Biophys Acta 1852:1428–1441 Available at: http://dx.doi.org/10.1016/j.bbadis.2015.03.015.

Naia L, Cunha-Oliveira T, Rodrigues J, Rosenstock TR, Oliveira A, Carmo C, Oliveira-sousa SI, Duarte AI, Hayden MR, Rego AC (2017) Histone Deacetylase Inhibitors Protect Against Pyruvate Dehydrogenase Dysfunction in Huntington's Disease. J Neurosci 37:2776–2794.

Nicoletti F, di Nuzzo L, Orlando R, Nasca C (2014) Molecular pharmacodynamics of new oral drugs used in the treatment of multiple sclerosis. Dovepress 8:555–568.

Oddo S, Caccamo A, Shepherd JD, Murphy MP, Golde TE, Kayed R, Metherate R, Mattson MP, Akbari Y, Laferla FM (2003) 3xTg-AD model of Alzheimer's disease with plaques and tangles_intracellular Aβ and synaptic dysfunction. Neuron 39:409–421.

Park M, Moon W (2016) Structural MR Imaging in the Diagnosis of Alzheimer's Disease and Other Neurodegenerative Dementia: Current Imaging Approach and Future Perspectives. Korean J Radiobiol 17:827–845.

Pérez-Corredor P, Sabogal-Guáqueta AM, Carrillo-Hormaza L, Cardona-Gómez GP (2019) Preventive Effect of Quercetin in a Triple Transgenic Alzheimer's Disease Mice Model. Molecules 24:1–10.

Perl DP (2010) Neuropathology of Alzheimer's Disease. Mt Sinai J Med 77:32–42.

Pietropaolo S, Feldon J, Yee BK (2008) Age-Dependent Phenotypic Characteristics of a Triple Transgenic Mouse Model of Alzheimer Disease. Behav Neurosci 122:733–747.

Pietropaolo S, Feldon J, Yee BK (2014) Environmental enrichment eliminates the anxiety phenotypes in a triple transgenic mouse model of Alzheimer's disease. Cogn Affect Behav Neurosci 14:996–1008.

Pirooznia SK, Elefant F (2013) Targeting specific HATs for neurodegenerative disease treatment : translating basic biology to therapeutic possibilities. Front Cell Neurosci 7:1–18.

Qing H, He G, Ly PTT, Fox CJ, Staufenbiel M, Cai F, Zhang Z, Wei S, Sun X, Chen C-H, Zhou W, Wang K, Song W (2008) Valproic acid inhibits Aβ production, neuritic plaque formation, and behavioral deficits in Alzheimer's disease mouse models. J Exp Med 205:2781–2789.

Qiu L, Tan EK, Zeng L (2015) microRNAs and Neurodegenerative Diseases. 888:85–105 Available at: http://link.springer.com/10.1007/978-3-319-22671-2.

Querfurth HW, LaFerla FM (2010) Alzheimer's Disease. N Engl J Med 362:329–344.

Raina AK, Templeton DJ, Deak JC, Perry G, Smith MA (2004) Quinone reductase (NQO1), a sensitive redox indicator, is increased in Alzheimer's disease. Redox Rep 4:23–27.

Reddy PH (2006) Mitochondrial oxidative damage in aging and Alzheimer's disease: Implications for mitochondrially targeted antioxidant therapeutics. J Biomed Biotechnol 2006:1–13.

Reitz C, Mayeux R (2014) Alzheimer disease: Epidemiology, Diagnostic Criteria, Risk Factors and Biomarkers. Biochem Pharmacol 88:640–651.

Ricobaraza A, Cuadrado-Tejedor M, Marco S, Pérez-Otaño I, García-Osta A (2010) Phenylbutyrate rescues dendritic spine loss associated with memory deficits in a mouse model of Alzheimer disease. Hippocampus 22:1040–1050.

Ricobaraza A, Cuadrado-Tejedor M, Pérez-Mediavilla A, Frechilla D, Del Río J, García-Osta A (2009) Phenylbutyrate ameliorates cognitive deficit and reduces tau pathology in an alzheimer's disease mouse model. Neuropsychopharmacology 34:1721–1732.

Saha RN, Pahan K (2006) HATs and HDACs in neurodegeneration: A tale of disconcerted acetylation homeostasis. Cell Death Differ 13:539–550.

Sanchez-Mut J V., Gräff J (2015) Epigenetic Alterations in Alzheimer's Disease. Front Behav Neurosci 9:1–17.

Santana I, Farinha F, Freitas S, Rodrigues V, Carvalho Á (2015) Estimativa da prevalência da demência e da doença de Alzheimer em Portugal. Acta Med Port 28:182–188.

Schipper HM, Cissé S, Stopa EG (1995) Expression of heme oxygenase-1 in the senescent and alzheimer-diseased brain. Ann Neurol 37:758–768.

Schneider A, Chatterjee S, Bousiges O, Selvi BR, Swaminathan A, Cassel R, Blanc F, Kundu TK, Boutillier AL (2013) Acetyltransferases (HATs) as Targets for Neurological Therapeutics. Neurotherapeutics 10:568–588.

Selkoe D, Schenk D (2003) Alzheimer's disease : Molecular Understanding Predicts Amyloid-Based Therapeutics. Annu Rev Pharmacol Toxicol 43:545–584.

Sengupta A, Wu Q, Grundke-Iqbal I, Iqbal K, Kabat J, Novak M (1998) Phosphorylation of tau at both Thr 231 and Ser 262 is required for maximal inhibition of its binding to microtubules. Arch Biochem Biophys 357:299–309.

Serrano-Pozo A, Frosch M, Masliah E, Hyman B (2011) Neuropathological alterations in Alzheimer disease. Cold Spring Harb Perspect Med 1:1–23.

Sharma S, Lu H-C (2018) microRNAs in Neurodegeneration: Current Findings and Potential Impacts Salil. J Alzheimers Dis Park 8:1–18.

Shi Q, Gibson GE (2007) Oxidative stress and transcriptional regulation in Alzheimer disease. Alzheimer Dis Assoc Disord 21:276–291.

Soares E, Prediger RD, Nunes S, Castro AA, Viana SD, Lemos C, De Souza CM, Agostinho P, Cunha RA, Carvalho E, Fontes Ribeiro CA, Reis F, Pereira FC (2013) Spatial memory impairments in a prediabetic rat model. Neuroscience 250:565–577 Available at: http://dx.doi.org/10.1016/j.neuroscience.2013.07.055.

Sova M, Saso L (2018) Design and development of Nrf2 modulators for cancer chemoprevention and therapy: A review. Dovepress 12:3181–3197.

Sterniczuk R, Antle MC, Laferla FM, Dyck RH (2010a) Characterization of the 3xTg-AD mouse model of Alzheimer's disease: Part 2. Behavioral and cognitive changes. Brain Res 1348:149–155 Available at: http://dx.doi.org/10.1016/j.brainres.2010.06.011.

Sterniczuk R, Dyck RH, LaFerla FM, Antle MC (2010b) Characterization of the 3xTg-AD mouse model of Alzheimer's disease: Part 1. Circadian changes. Brain Res 1348:139–148 Available at: https://linkinghub.elsevier.com/retrieve/pii/S0006899310010929.

Stover KR, Campbell MA, Van Winssen CM, Brown RE (2015) Early detection of cognitive deficits in the 3xTg-AD mouse model of Alzheimer's disease. Behav Brain Res 289:29–38 Available at: http://dx.doi.org/10.1016/j.bbr.2015.04.012.

Sumner IL, Edwards RA, Asuni AA, Teeling JL (2018) Antibody engineering for Optimized immunotherapy in Alzheimer's disease. Front Neurosci 12:1–12.

Sun J, Wang F, Li H, Zhang H, Jin J, Chen W, Pang M, Yu J, He Y, Liu J, Liu C (2015) Neuroprotective Effect of Sodium Butyrate against Cerebral Ischemia/Reperfusion Injury in Mice. Biomed Res Int 2015:1–8.

Sun Y, Yang T, Mao L, Zhang F (2017) Sulforaphane Protects against Brain Diseases: Roles of Cytoprotective Enzymes. Austin J Cerebrovasc Dis Stroke 4:1–17.

Sun Z, Huang Z, Zhang DD (2009) Phosphorylation of Nrf2 at multiple sites by MAP kinases has a limited contribution in modulating the Nrf2-dependent antioxidant response. PLoS One 4:1–9.

Swerdlow R (2007) Pathogenesis of Alzheimer's Disease. Clin Interv Aging 2:347–359.

Taipa R, Pinho J, Melo-Pires M (2012) Clinico-pathological correlations of the most common neurodegenerative dementias. Front Neurol 3:1–13.

Tandon N, Ramakrishna V, Kumar SK (2016) Clinical use and applications of histone deacetylase inhibitors in multiple myeloma. Dovepress 8:35–44.

Tarawneh R, Holtzman DM (2012) The clinical problem of symptomatic Alzheimer disease and mild cognitive impairment. Cold Spring Harb Perspect Med 2:1–16.

Torre JC de la (2012) Cardiovascular Risk Factors Promote Brain Hypoperfusion Leading to Cognitive Decline and Dementia. Cardiovasc Psychiatry Neurol 2012:1–15.

Torres-Lista V, Parrado-Fernández C, Alvarez-Montón I, Frontiñán-Rubio J, Durán-Prado M, Peinado JR, Johansson B, Alcaín FJ, Giménez-Llort L (2014) Neophobia, NQO1 and SIRT1 as premorbid and prodromal indicators of AD in 3xTg-AD mice. Behav Brain Res 271:140–146.

Tseng B, Green K, Chan J, Blurton-Jones Ma, LaFerla F (2008) Aβ inhibits the proteasome and enhances amyloid and tau accumulation. Neurobiol Aging 29:1607–1618 Available at: http://linkinghub.elsevier.com/retrieve/pii/014067369290865Z.

Vasconcelos AR, dos Santos NB, Scavone C, Munhoz CD (2019) Nrf2/ARE Pathway Modulation by Dietary Energy Regulation in Neurological Disorders. Front Pharmacol 10:1–18.

Vogel-Ciernia A, Wood MA (2014) Examining object location and object recognition memory in mice. Curr Protoc Neurosci 8:8.31.1-8.31.17.

Walls K, Ager R, Vasilevko V, Cheng D, Medeiros R, LaFerla F (2014) p-Tau immunotherapy reduces soluble and insoluble tau in aged 3xTg-AD mice. Neurosci Lett 575:96–100.

Xu K, Dai X-L, Huang H-C, Jiang Z-F (2011) Targeting HDACs: A Promising Therapy for Alzheimer's Disease. Oxid Med Cell Longev 2011:1–5.

Yamamoto H, Hiragami Y, Murayama M, Ishizuka K, Kawahara M, Takashima A (2005) Phosphorylation of tau at serine 416 by Ca2+/calmodulin- dependent protein kinase II in neuronal soma in brain. J Neurochem 94:1438–1447.

Yang S shuang, Zhang R, Wang G, Zhang Y fang (2017) The development prospection of HDAC inhibitors as a potential therapeutic direction in Alzheimer's disease. Transl Neurodegener 6:1–6.

Yin Y, Morgunova E, Jolma A, Kaasinen E, Sahu B, Khund-Sayeed S, Das PK, Kivioja T, Dave K, Zhong F, Nitta KR, Taipale M, Popov A, Ginno PA, Domcke S, Yan J, Schübeler D, Vinson C, Taipale J (2017) Impact of cytosine methylation on DNA binding specificities of human transcription factors. Science (80-) 356:1–15.

Yoshida M, Kikima M, Akita M, Beppu T (1990) Potent and specific inhibition of mammalian in vivo and in vitro by trichostatin A. J Biol Chem 265:17174–17179.

Zhang ZY, Schluesener HJ (2013) Oral administration of histone deacetylase inhibitor MS-275 Ameliorates neuroinflammation and cerebral amyloidosis and improves behavior in a mouse model. J Neuropathol Exp Neurol 72:178–185.

Zovkic IB, Guzman-Karlsson MC, Sweatt JD (2013) Epigenetic regulation of memory formation and maintenance. Learn Mem 20:61–74.

Zuo L, Hemmelgarn BT, Chuang C-C, Best TM (2015) The Role of Oxidative Stress-Induced Epigenetic Alterations in Amyloid- β Production in Alzheimer's Disease . Oxid Med Cell Longev 2015:1–13.

Zwergel C, Stazi G, Valente S, Mai A (2016) Histone Deacetylase Inhibitors: Updated Studies in Various Epigenetic-Related Diseases. J Clin Epigenetics 2:1–15.